An Investigation Into the Use of Orthogonal Winding in Loosely Coupled Link for Improving Power Transfer Efficiency Under Coil Misalignment

Jeff Po Wa Chow, *Student Member, IEEE*, Nan Chen, *Member, IEEE*,
Henry Shu Hung Chung, *Senior Member, IEEE*, and Leanne Lai Hang Chan, *Member, IEEE*

***Abstract*—It is sometimes unavoidable to use loosely coupled coils in applications, like biomedical devices, for transferring electric energy wirelessly. However, coil misalignment causes degradation of the power transfer efficiency. It is well known that the power transfer efficiency of classical parallel coils is primarily determined by the quality factors of the coils and the coupling coefficient between the coils, and is maximized by choosing an optimal turns-ratio between the coils. Changing the number of turns of the coils cannot effectively overcome such misalignment effect. This paper presents a structure that comprises two orthogonally placed windings for lessening the variation of the coupling coefficient due to the coil misalignment. An output current summing technique that keeps the windings concurrently energized and combines the output currents of the windings will be studied. A canonical model will also be derived to describe the interactions between the coils. An experimental prototype has been built and evaluated on a test bed, which allows different degrees of lateral and angular misalignments. Results reveal that the proposed structure can effectively increase the minimum efficiency zone, allowing more lateral and angular misalignments. These investigations lay the foundation for future understanding more complex loosely coupled winding structures.**

***Index Terms*—Coil misalignments, winding structure, wireless inductive link, wireless power transfer.**

I. Introduction

WIRELESS inductive links have been widely used in many applications, such as cochlear implants [1], retinal prostheses [2]–[4], battery chargers [5], transportation [6], [7], and induction heating [8]. They are generally composed of a transmitter, an end-use device, and two coils with one coil in the transmitter and another one in the end-use device. As some applications, such as biomedical applications, do not allow using any ferromagnetic core, the two coils are loosely coupled. The transmitter and receiver coils are typically placed in parallel. Electric energy is transmitted from the transmitting coil to the receiving coil through alternating magnetic fields. The system is optimized toward maximum power transfer efficiency [9]–[12]. Although many improved transmitter and receiver designs have emerged, the link efficiency is still determined by a fundamental "bottleneck"—fluctuations in the power transfer and link efficiency due to the coil misalignment. When the coils are coaxially orientated, the coils are well coupled and thus the link efficiency is maximal. However, if the two coils are misaligned, the magnetic coupling and the overall link efficiency will impair.

As discussed in [9], the maximum power transfer efficiency of parallel placed coils is dependent on the coil quality factors, as defined in (E10), and the coupling coefficient between the two coils, as defined in (35) and (36). The coupling coefficient gives measure of the degree of magnetic coupling, determined by the coil sizes and geometric spacing. When the coils are coaxially orientated, their coupling is the strongest. However, the coils could be misaligned axially, laterally, and angularly in practical situations, impairing their magnetic coupling [13]. Take retinal prosthesis utilizing wireless telemetry for power transfer as an example, axial and lateral misalignment would occur upon displacement of the pair of glasses [3]. More importantly, impairment of magnetic coupling, due to the coil misalignment [13]–[15], can lead to reduction of power efficiency. There is a rule of thumb in maximizing misalignment tolerance for disk-shaped primary coil. The primary coil diameter should be larger than that of secondary coil and equal to twice the distance between two coils [14], [16]. However, there are concerns with this design approach. First, the volt–amp rating of the transmitter is nonoptimal, as the variation of the coupling coefficient is large and a large portion of magnetic flux generated by the transmitter is uncoupled to the secondary coil, no matter under aligned or misaligned condition. Second, a large portion of magnetic flux is transmitted to free space. Third, the coils have to be oversized in order to improve the misalignment tolerance.

There are structures having multiple windings in the transmitter and/or receiver [5], [17]–[25] for different operational targets. The methods discussed in [5] and [17] have multiple

Manuscript received June 28, 2014; revised October 6, 2014; accepted November 6, 2014. Date of publication November 25, 2014; date of current version May 22, 2015. This work was supported by a grant from the Research Grants Council of the Hong Kong Special Administrative Region, China, through Project CityU 112613 and also under the program for professor of special appointment (Eastern Scholar) at Shanghai Institutions of Higher learning. This paper was presented in part at the 35th Annual International Conference of the IEEE Engineering in Medicine and Biology Society, Osaka, Japan, July 3–7, 2013 and will be in part presented at the IEEE Energy Conversion Congress and Exposition 2014, Pittsburgh, PA, USA. Recommended for publication by Associate Editor J. Biela.

J. P. W. Chow and L. L. H. Chan are with the Centre for Smart Energy Conversion and Utilization Research, City University of Hong Kong, Kowloon, Hong Kong (e-mail: pwchow2-c@my.cityu.edu.hk; lhlchan@cityu.edu.hk).

N. Chen is with the ABB Corporate Research Center, Västerås 72178, Sweden (e-mail: nan.chen@se.abb.com).

H. S. H. Chung is with the Centre for Smart Energy Conversion and Utilization Research, City University of Hong Kong, Kowloon, Hong Kong and is also with Research Institute of Electronic Automation, Shanghai Maritime University, Shanghai 201306, China (e-mail: eeshc@cityu.edu.hk).

Color versions of one or more of the figures in this paper are available online at http://ieeexplore.ieee.org.

Digital Object Identifier 10.1109/TPEL.2014.2374651

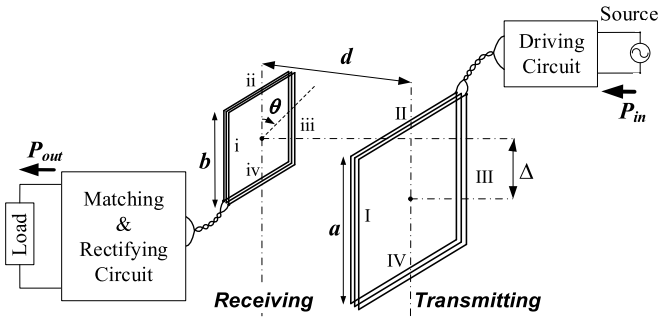

Fig. 1. Wireless inductive link with square-shaped loosely coupled coils.

displaced parallel transmitter coils to establish a near-uniform perpendicular flux around the receiver coil. Due to the confined flux direction, the coupling method is specifically used to tackle lateral misalignment. The 3-D structure discussed in [18] and [19] offers an omnidirectional coupling. Three windings in the receiver are placed orthogonally. Each winding is resonated by a parallel capacitor and its output is rectified by a diode circuit. Then, the rectified outputs are paralleled [26], [27]. As discussed in [19], since the three voltage outputs are in parallel, it can only allow a narrow operation region to simultaneously energize all windings. Thus, the worst-case scenario is that only one of the three windings in the structure delivers output power. It is effectively a single-coil-to-single-coil coupling, and thus cannot guarantee to operate at the achievable maximum power transfer. The methods discussed in [20]–[22] utilize resonator coils to maximize power transfer in a relatively longer distance under an aligned condition. The added extra winding in [23] functions as a data coil for communication.

To attain a high-level magnetic coupling under misaligned conditions, this paper provides a new perspective and detailed investigation into the use of *parallel* and *orthogonal* windings in the receiving coil set for loosely coupled link. An output current summing technique, based on using an inductor to form a current source at the output of the rectifier, is proposed to broaden the range of possible misalignments where the secondary coils are energized. For the sake of simplicity in the analysis and illustration, two orthogonally placed windings, instead of three as discussed in [18] and [19], are studied.

The performance of an experimental prototype with two coil sets, including the classical parallel coil structure and the proposed structure, will be evaluated. The experimental results are favorably compared to the theoretical predictions. The conclusions follow in the last section.

II. Motivation

The wireless inductive link with square-shaped loosely coupled coils is illustrated in Fig. 1. The power transfer efficiency versus the number of turns in the receiving coil will be studied further on in this paper theoretically and experimentally. The parameters of the 16-turn transmitting coil used in the study are given in Table I. Five receiving coils having 6, 12, 18, 24, and 36 turns, respectively, are fabricated, in order to study the transfer efficiency, which is defined as the ratio between the load power $P_{\rm out}$ and the power supplied to the transmitting coil $P_{\rm in}$. Fig. 2 shows the results when the coils are under three testing cases—aligned and two misaligned conditions. For the sake of comparison, the load resistor and the resonant capacitors for the transmitting and receiving coils, respectively, are designed such that maximum power transfer efficiency occurs in all cases. The theoretical analysis is based on the method described in [9]. Several nonideal characteristics, such as the power loss in the diode-bridge rectifier, winding resistance, etc., are taken into account. Results reveal that the efficiency is increased when the number of turns is increased from 6 turns to 12 turns. Then, it becomes fairly constant, even if the number of turns is increased to 36 turns. It is mainly because the ac resistance of the coils increases with the increase in the number of turns, due to the proximity effect [28]. Such resistive effect becomes dominant and gives an adverse effect on the efficiency, even if the flux linkage between the transmitting and receiving coils is also increased with the increased number of turns. The study concludes that the maximum efficiency is primarily determined by the quality factors of the coils and the coupling coefficient between the coils. The efficiency variations versus the number of turns in the three testing cases are similar, demonstrating that variation of the transfer efficiency, due to coil misalignment, cannot be overcome effectively by simply changing the number of turns in the receiving coil.

A T-shaped structure with two orthogonally placed windings, as shown in Fig. 3, is investigated. It is composed of two windings, namely *parallel* and *orthogonal* windings which are similar to the cross-shaped structure presented in [29]. The

TABLE I
Parameters of the Transmitting Coil Used in the Experiment.

a (cm)	N_1^*	L_1 (μH)	r_1 (Ω)†	C_1 (pF)	d (cm)	f (MHz)	Wire size (AWG)
4	16	27.0	5.4	195	2	2.2	28

$*N_1$: Number of turns of transmitting coil.
$^\dagger r_1$: AC resistance of the coil at the operating frequency f.

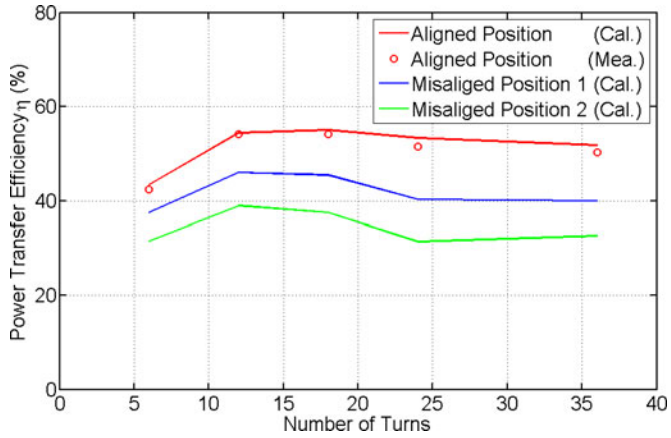

Fig. 2. Power transfer efficiency versus number of turns in the receiving coil.

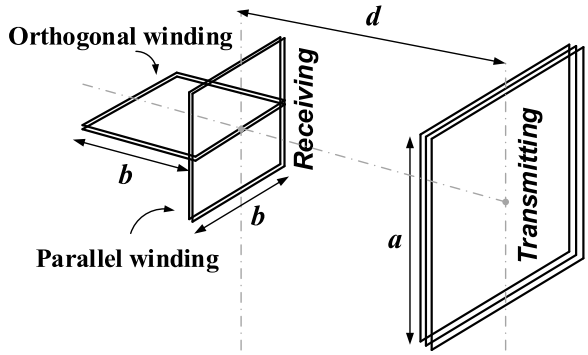

Fig. 3. Proposed winding structure with a parallel winding and an orthogonal winding.

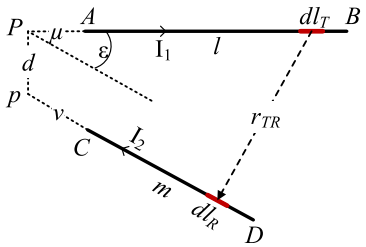

Fig. 4. Mutual inductance of two filaments.

T-shaped structure makes the parallel winding deliver more power as the parallel winding is placed closer to the transmitting coil for the same axial separation between the two coils. The parallel winding has the same number of turns as the optimal number of turns in the parallel coil structure, i.e., 12 turns in the case study. The orthogonal winding is used to assist with increasing the flux linkage between the coils under the misaligned condition. Extensive mathematical treatment and investigations into the power transfer phenomenon of the T-shaped structure will be conducted in the following sections.

III. Mutual Inductance Between Coils

A. Formulation of the Mutual Inductance

In order to study the effect of misalignment on affecting the power transfer efficiency, the following investigations start with calculating the mutual inductance and magnetic field distribution between the coils. The mutual inductance is defined as the number of flux linkages with the secondary coil due to unit current in primary coil. It is determined by the double integral Neumann formula [30]:

$$M = \frac{\mu_0}{4\pi} \oint_T \oint_R \frac{dl_T\, dl_R}{r_{TR}} \cos\varepsilon \tag{1}$$

where dl_T and dl_R are the infinitesimal segments of the transmitting coil and receiving coil, respectively, and r_{TR} and ε are the distance and angle between the two segments, respectively. Equation (1) is applicable for different shapes of coils.

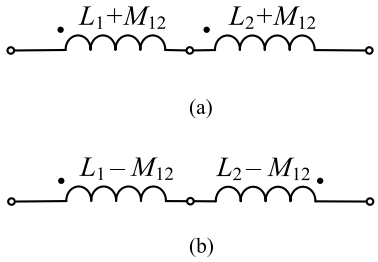

Fig. 5. Connections of the two coils for measuring mutual inductance. (a) SAM. (b) SOM.

The mutual inductance M_f between two filaments of lengths l and m, respectively, as shown in Fig. 4 is [30]

$$M_f = \operatorname{sgn}(\hat{I}_1 \cdot \hat{I}_2) 0.001 \cos\varepsilon \left\{ 2\left[(\mu + l)\tanh^{-1}\frac{m}{R_1+R_2} + (\nu+m)\tanh^{-1}\frac{l}{R_1+R_4} - \mu\tanh^{-1}\frac{m}{R_3+R_4} - \nu\tanh^{-1}\frac{l}{R_2+R_3}\right] - \frac{\Omega d}{\sin\varepsilon}\right\} \tag{2}$$

where $\hat{I}_1$ and $\hat{I}_2$ are the current unit vectors of filament AB and CD, respectively, $\operatorname{sgn}(\hat{I}_1 \cdot \hat{I}_2)$ is the sign of the dot product between $\hat{I}_1$ and $\hat{I}_2$. The mathematical expressions of the parameters are given in Appendix A.

In the following discussion, the coils shown in Fig. 1 are illustrated. Both the transmitting and receiving coils have four sets of wires having the same spatial orientation. They are sets I–IV in the transmitting coil, and sets i–iv in the receiving coil. The mutual inductance M_{12} between the transmitting coil and the receiving coil is calculated by summing up the mutual inductances of each set of wires in the transmitting coil with all other sets in the receiving coil. Thus

$$M_{12} = N_1\, N_2 \sum_{i=\mathrm{I}}^{\mathrm{IV}} \sum_{j=\mathrm{i}}^{\mathrm{iv}} M_{f,ij} \tag{3}$$

where N_1 and N_2 are numbers of turns of the transmitting coil and receiving coil, respectively, and $M_{f,ij}$ is the mutual inductance between a wire in the *i*th set in the transmitting coil and a wire in the *j*th set in the receiving coil.

B. Measurement of the Mutual Inductance Between Coils

The mutual inductance between two coupled coils is determined by measuring the self-inductance of each coil, and the total inductances when the two coils are connected in series. As illustrated in Fig. 5, there are two possible modes of connection: 1) series-aiding mode (SAM); and 2) series-opposing mode (SOM). In SAM, the magnetic fields generated by the coils are aided each other. The total inductance L_{SAM} is

$$L_{\mathrm{SAM}} = L_1 + L_2 + 2M_{12} \tag{4}$$

TABLE II
PARAMETERS OF THREE SETS OF RECEIVING COILS

b (cm)	$N_2 : N_3{}^*$	L_2 (μH)	r_2 (Ω)	C_2 (pF)	L_3 (μH)	r_3 (Ω)	C_3 (pF)	Wire size (AWG)
2.0	12:0	5.9	1.88	887	–	–	–	28
2.0	12:6	5.9	1.88	887	1.73	0.51	3000	28
2.1	12:24	5.9	1.88	887	29.91	9.91	185	28

$^*N_2$ and N_3 are the number of turns of parallel winding and orthogonal winding, respectively.

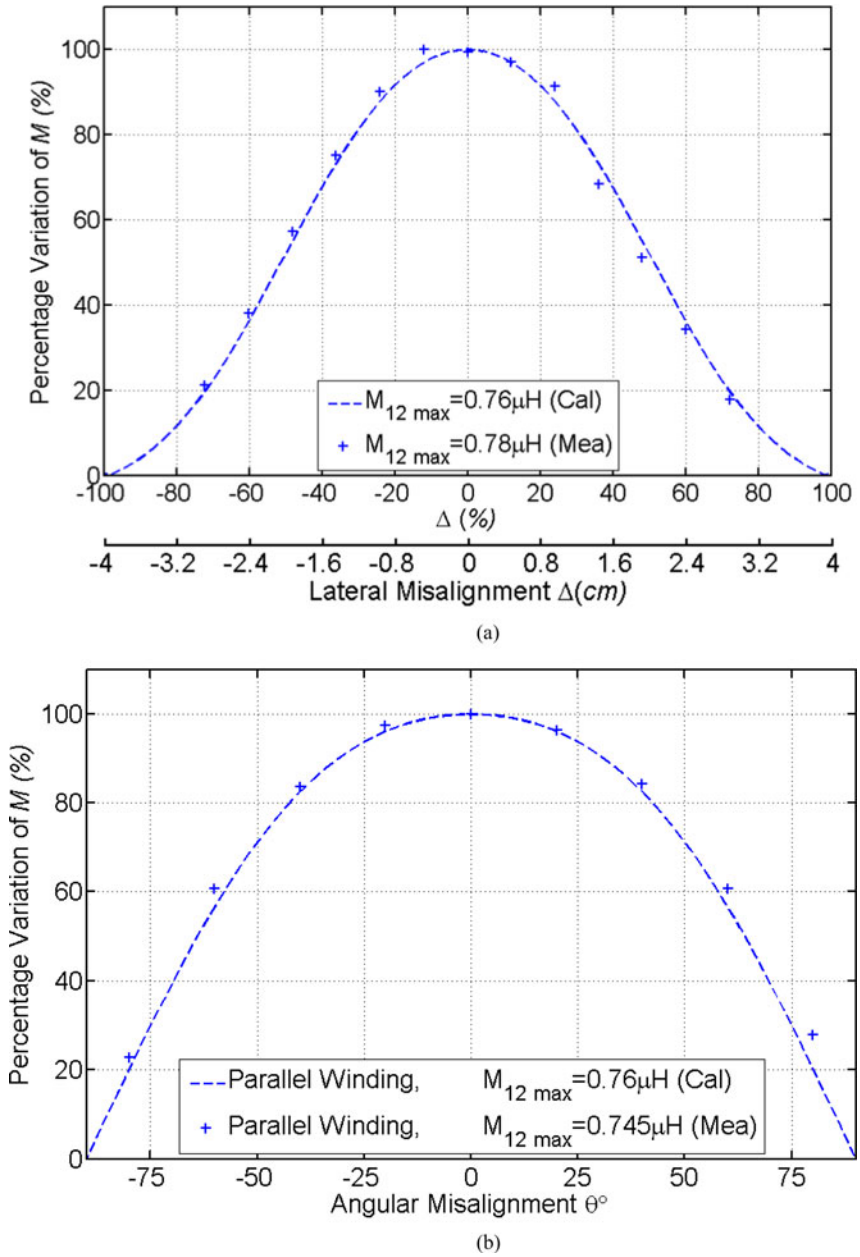

Fig. 6. Mutual inductance under lateral and angular misalignments. (a) Lateral misalignment. (b) Angular misalignment.

where L_1 and L_2 are the self-inductances of the transmitting and receiving coils, respectively, and M_{12} is the mutual inductance between the two coils.

Conversely, in SOM, the magnetic fields generated by the coils are opposed to each other. The total inductance L_{SOM} is

$$L_{\mathrm{SOM}} = L_1 + L_2 - 2M_{12}. \tag{5}$$

By using (4) and (5), M_{12} can be determined by the measured values of L_1 and L_2, $L_{\rm SAM}$, and $L_{\rm SOM}$ using the formulas of

$$M_{12} = \frac{1}{2}(L_{\rm SAM} - L_1 - L_2) \tag{6}$$

or

$$M_{12} = \frac{1}{2}(L_1 + L_2 - L_{\rm SOM}). \tag{7}$$

C. Mutual Inductance Under Lateral and Angular Misalignments

When the centers of the transmitting and receiving coils are aligned, their mutual inductance is maximal. However, it is practically unavoidable to have coil misalignments. In this section, variations of their mutual inductance under lateral and angular misalignments are studied. Fig. 1 illustrates a general case where the coils are misaligned. Let *d* be the distance between the centers of the two coils under perfectly aligned condition, Δ be the lateral displacement between the centers of the two coils under lateral misalignment, and θ be the angle between the planes of the two coils under angular misalignment. Based on the parameters given in Tables I and II, Fig. 6(a) and (b) shows the calculated and measured mutual inductance M_{12} under lateral misalignment Δ with $\theta = 0$ and angular misalignment θ with $\Delta = 0\%$, respectively. The calculations are based on the equations given in (1)–(3), while the measurements are conducted by the method described in Section III-B.

When the two coils are perfectly aligned, i.e., Δ and θ are both zero, M_{12} is the highest. M_{12} reduces with an increase in any misalignment. As shown in Fig. 6, under a lateral misalignment of 50% relative to the length of the transmitting coil, M_{12} is reduced by 50%. Under an angular misalignment of 45°, M_{12} is reduced by 20%. The value of M_{12} will decrease more rapidly as the angular misalignment is further increased. The coupling becomes zero at the maximum misalignment. With the help of Fig. 7(a), the reduction in M_{12} can be visualized by considering the flux linkage between the two coils under various misaligned conditions. For the sake of simplicity, only lateral misalignment is illustrated. Assume that the position of the transmitting coil is fixed and the position of the receiving coil is movable. The flux linkage between the two coils is maximal when the plane of the receiving coil is perpendicular to the magnetic flux. At position "1," the orientation of the receiving coil is the best. As the receiving coil is displaced from position "1" to "4," the magnetic flux becomes not perpendicular to the plane of the transmitting coil anymore, but emanates outward. Thus, the flux linkage is diminished, as the coil is approaching to the edge of transmitting coil. Fig. 7(b) shows the desired orientation of the receiving coil at the four positions. At position "1," the receiving coil should be placed in parallel with the transmitting coil. As the position is moving toward the edge of the transmitting coil, the receiving coil should be rotated in order to pick up maximum magnetic flux. At position "4," it should be placed nearly orthogonal to the transmitting coil. Therefore, parallel coil can pick up more flux near the center of the transmitting coil, while orthogonal coil can pick up more flux near the edge of the transmitting coil.

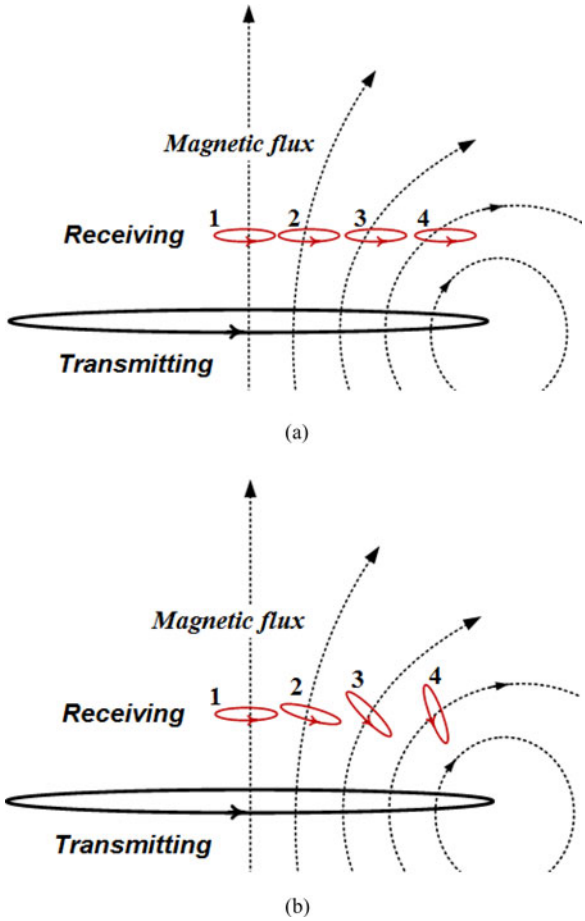

Fig. 7. Visualization of the flux linkage under the misaligned condition. (a) Illustration of the flux linkage under lateral misalignments. (b) Desired orientation of the receiving coil for maximum flux linkage.

D. Mutual Inductances of the Proposed Structure

Based on the previous observation, the T-shape receiving coil structure shown in Fig. 3 is investigated to tackle the reduction of the mutual inductance under coil misalignments. One end of the added orthogonal winding is aligned on the same plane of the parallel winding, so that the space between the transmitting coil and the proposed receiving coil is the same as the parallel-coil structure in Fig. 1. Without loss of generality, the two windings are assumed to have the same dimensions. Let M_{12} be the mutual inductance between the transmitting coil and the parallel winding, and M_{13} be the mutual inductance between the transmitting coil and the orthogonal winding. It should be noted that there is no inductive coupling between the parallel winding and the orthogonal winding as the two windings are spatially orthogonal. Fig. 8(a) and (b) shows the profiles of M_{12} and M_{13} under lateral misalignment with $\theta = 0$ and angular misalignment with $\Delta = 0\%$, respectively. The number of turns of the orthogonal winding is twice that of the parallel winding. When the receiving coil is perfectly aligned with the transmitting coil, M_{12} is maximized and M_{13} is zero. When the receiving coil is displaced, M_{12} drops but M_{13} increases. It should be noted that the polarity of the orthogonal windings is interchanged when Δ is negative.

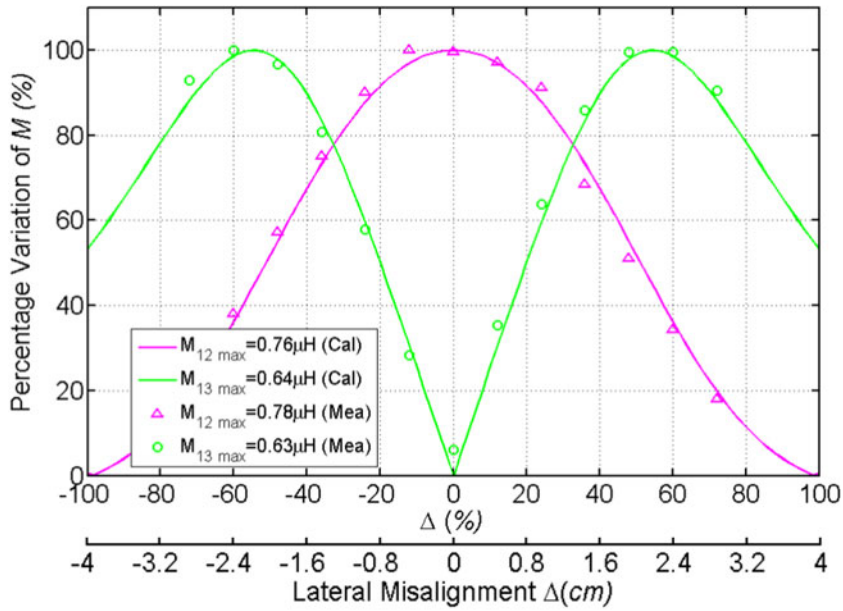

(a)

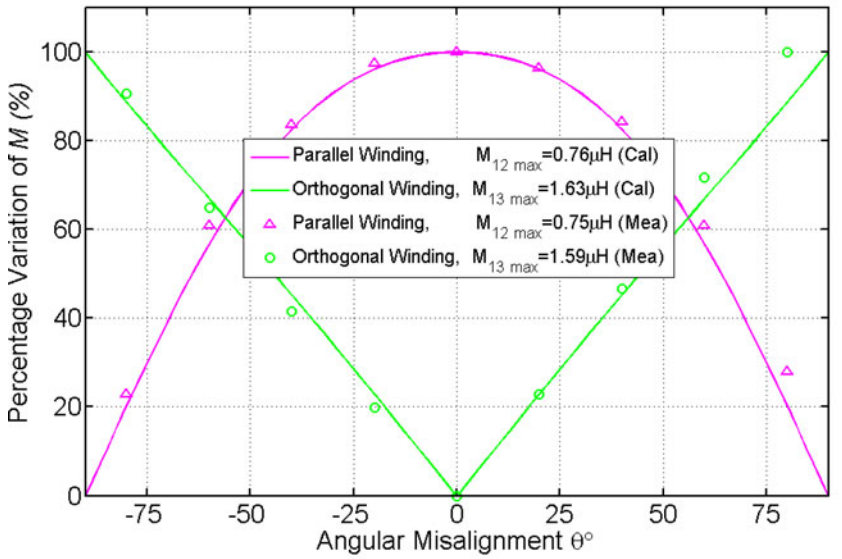

(b)

Fig. 8. Mutual inductance under lateral and angular misalignments. (a) Lateral Misalignment. (b) Angular misalignment.

IV. Modeling and Circuit Implementation

In order to maximize the utilization of the two windings in the power transfer, they are energized concurrently by using a current summing circuit. Such structure is studied by first modeling the windings with a proposed canonical transformer model and then applying it to develop a circuit model to study the overall power transfer phenomena.

A. Derivation of Canonical Transformer Model

A canonical transformer model that describes the interaction between the primary and secondary windings is derived. Fig. 9(a) shows the classical transformer model, in which the numerals "1" and "2" appeared in the subscripts denote the primary and secondary sides of the transformer, respectively. *L* and *r* are the self-inductance and resistance of the respective winding, respectively. The two windings have the turns ratio n_{12} and mutual inductance M_{12}. Based on Fig. 9(a), the following Laplace-transformed equations can be derived:

$$\begin{bmatrix} V_1(s) \\ V_2(s) \end{bmatrix} = \begin{bmatrix} sL_1 + r_1 & -sM_{12} \\ sM_{12} & -(sL_2 + r_2) \end{bmatrix} \begin{bmatrix} I_1(s) \\ I_2(s) \end{bmatrix}. \quad (8)$$

Equation (8) is rearranged to derive a canonical model as follows:

$$V_1(s) = \left[Z_1(s) + \frac{sn_{12}^2 M_{12} Z_2(s)}{n_{12} Z_2(s) + sM_{12}} \right] I_1(s) + n_{12} V_{d2}(s) \quad (9)$$

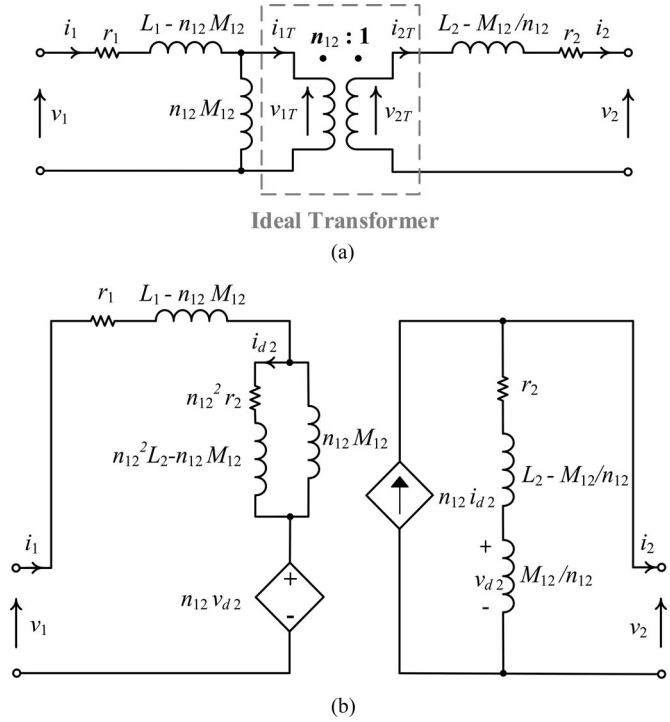

Fig. 9. Equivalent circuit of a transformer. (a) Classical model. (b) Canonical model.

$$I_2(s) = n_{12} I_{d2}(s) - \frac{1}{Z_2 + s\frac{M_{12}}{n_{12}}} V_2(s) \tag{10}$$

where

$$I_{d2}(s) = \frac{sM_{12}}{n_{12}(r_2 + sL_2)} I_1(s)$$

$$V_{d2}(s) = \frac{s\frac{M_{12}}{n_{12}}}{r_2 + s\left(L_2 - \frac{M_{12}}{n_{12}}\right) + s\frac{M_{12}}{n_{12}}} V_2(s)$$

$$Z_1(s) = r_1 + s(L_1 - n_{12}M_{12})$$

and

$$Z_2(s) = r_2 + s\left(L_2 - \frac{M_{12}}{n_{12}}\right)$$

.

Derivations of (9) and (10) are given in Appendix B. Equation (9) describes the primary (input)-side circuit with a voltage-dependent voltage source $n_{12}\ v_{d2}$ in series with Z_1 and a parallel impedance of $n_{12}^2 Z_2$ and $s\ n_{12} M_{12}$. Equation (10) describes the secondary (output)-side circuit with a current-dependent current source $n_{12}\ i_{d2}$ in parallel with a series *RL* circuit, formed by the impedances Z_2 and $s\ \frac{M_{12}}{n_{12}}$. Fig. 9(b) shows the canonical transformer model.

B. Circuit Implementation With Current Summing Technology

As mentioned in Section III-D, the connections between the parallel and the orthogonal windings should be interchanged, when the polarity of the lateral and angular misalignments are reversed. The circuit structure shown in Fig. 10(a) performs such function. The numerals "1," "2," and "3" appeared in the subscripts denote the transmitting coil, parallel winding, and orthogonal winding in the receiving coil, respectively. A capacitor C_1 is connected in series with the transmitting coil to resonate with the self-inductance L_1 of the coil [11], [31], so as to eliminate the effect of the series inductance and thus maximize the input power. Each output winding has a diode bridge connected. Fig. 10(b) illustrates how the canonical transformer model is applied. The outputs of the windings are current sources $n_{12}\ i_{d2}$ and $n_{13}\ i_{d3}$. Thus, in order to extract maximum currents from the windings, parallel resonant capacitors C_2 and C_3 are used. Such parallel resonance can also amplify the output voltages $v_{\rm out2}$ and $v_{\rm out3}$ to minimize the decrement of the efficiency caused by the forward voltage drop of the diode bridges. Since the phases of the output currents $i_{\rm out2}$ and $i_{\rm out3}$ are dependent on the ratio between the load impedance and the output parallel *LC* impedance, they can be of different values. Thus, if the outputs of the diode bridges are connected together, only a small phase difference between $i_{\rm out2}$ and $i_{\rm out3}$ can lead to circulating current and result in deenergizing one of the winding outputs. Thus, series inductors $L_{\rm rect2}$ and $L_{\rm rect3}$ with equivalent series resistances $r_{\rm rect2}$ and $r_{\rm rect3}$, respectively, are connected to the outputs of the diode bridges in order to energize both windings and deliver rectified and smooth output currents $I_{\rm rect2}$ and $I_{\rm rect3}$. Then, the outputs of the inductors are connected to the load R_L together.

C. Operating Modes of the Proposed Structure

As the mutual inductances M_{12} and M_{13} vary with the misalignment condition, there are three possible modes of operation, in which both windings or only one of the windings feed electric energy to the load. The equivalent circuits of the three modes are shown in Fig. 10(b)–(d). The operations are discussed as follows.

1) *Mode 1—Both windings transferring energy to the load:* In this mode, both windings process the energy transferred to the load. Fig. 10(b) shows the equivalent circuit model. The forward voltage drop of the diodes in the parallel and orthogonal windings is V_{D2} and V_{D3}, respectively. The output voltages of the windings, $v_{\rm out2}$ and $v_{\rm out3}$, can be expressed as

$$v_{\rm out3} \approx \frac{H_2 v_{\rm out2} - H_1 v_{\rm in} - 2(V_{D2} - V_{D3})}{H_3} \tag{12}$$

where $C_1 = \frac{1}{\omega^2 L_1}, C_2 = \frac{1}{\omega^2 L_2}, C_3 = \frac{1}{\omega^2 L_3}$, and ω is the angular operating frequency.

$$v_{\rm out2} \approx \frac{\left[H_4 + \frac{H_1}{H_3}(Y_{rc3} + K_3 H_4)\right] v_{\rm in} + \frac{8}{\pi R_L} V_{D2} + \frac{2(Y_{rc3} + K_3 H_4)}{H_3}(V_{D2} - V_{D3})}{\frac{8}{\pi^2 R_L} + Y_{rc2}\left(1 + \frac{r_{\rm rect2}}{R_L}\right) + Y_{rc3}\frac{H_2}{H_3} + \frac{(K_2 H_3 + K_3 H_2) H_4}{H_3}} \tag{11}$$

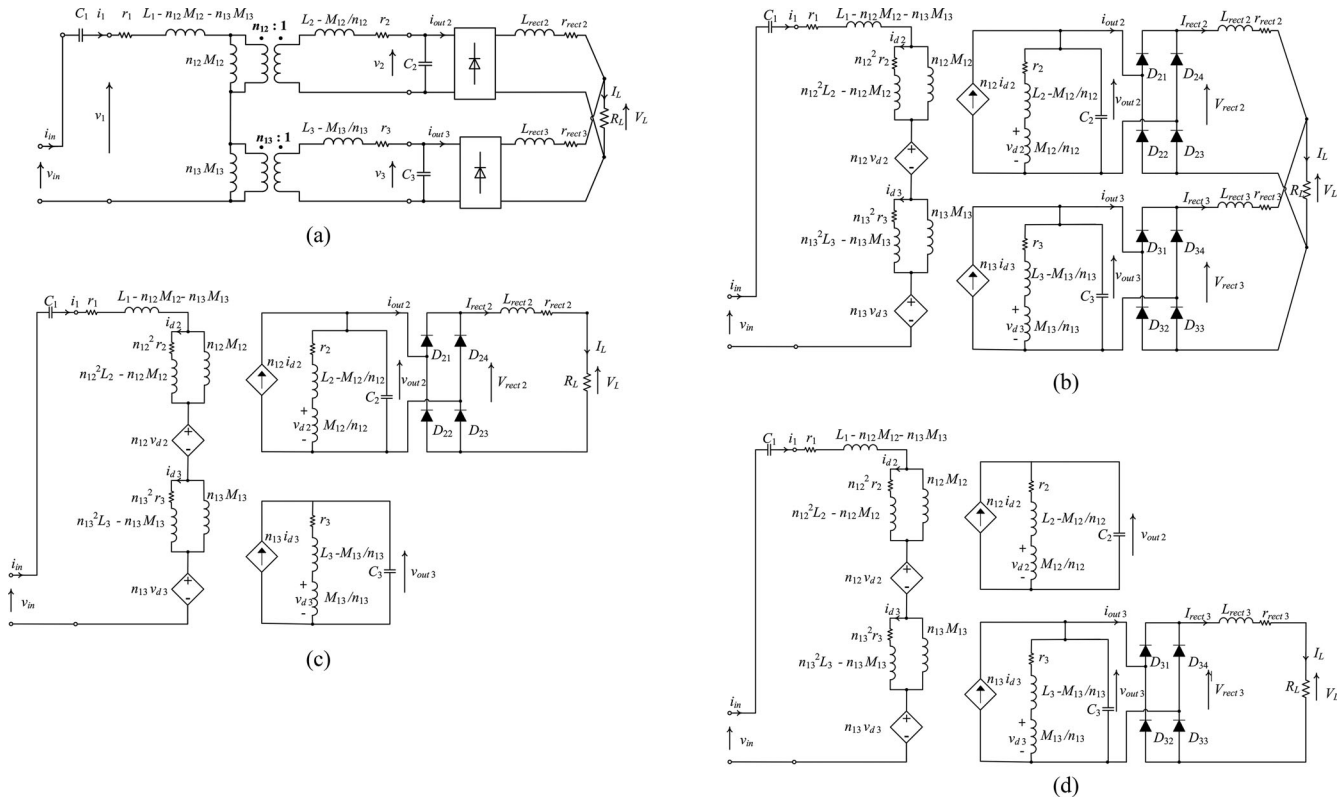

Fig. 10. Circuit implementation and equivalent circuits in the three operating modes. (a) Proposed circuit implementation. (b) Equivalent circuit in Mode 1 operation. (c) Equivalent circuit in Mode 2 operation. (d) Equivalent circuit in Mode 3 operation.

Derivations of (11) as shown bottom of the previous page and (12), and definition of the parameters are given in Appendix C. If the dc resistances of the series inductors, $r_{\rm rect2}$ and $r_{\rm rect3}$, are much smaller than the load resistance R_L, and V_{D2} and V_{D3} are assumed to be the same, $r_{\rm rect2} = r_{\rm rect3} = 0$ and $V_{D2} = V_{D3} = V_D$. Equations (11) and (12) can be simplified as

$$v_{\rm out2} \approx \frac{\frac{K_2+K_3}{K_1} v_{\rm in} + \frac{8}{\pi R_L} V_D}{\frac{8}{\pi^2 R_L} + Y_{rs2} + Y_{rs3} + \frac{(K_2+K_3)^2}{K_1}} \tag{13}$$

$$v_{\rm out3} = v_{\rm out2} = v_{\rm out}. \tag{14}$$

The average load voltage V_L and the input current $i_{\rm in}$ are

$$V_L = \frac{2}{\pi} V_{\rm out,pk} - 2V_D \tag{15}$$

$$i_{\rm in} = \frac{v_{\rm in} - (K_2+K_3) v_{\rm out2}}{K_1} \tag{16}$$

where $V_{\rm out,pk}$ is the amplitude of $v_{\rm out}$.

2) *Mode 2—Only parallel winding transferring energy to the load:* This mode occurs when the transmitting coil and the parallel winding are near to the aligned condition. Fig. 10(c) shows the equivalent circuit model. $v_{\rm out2}$ and $v_{\rm out3}$ can be expressed as

$$v_{\rm out2} \approx \frac{\frac{K_2 Y_{rc3}}{K_1 Y_{rc3} + K_3^2} v_{\rm in} + \frac{8}{\pi (R_L + r_{\rm rect2})} V_D}{\frac{8}{\pi^2 (R_L + r_{\rm rect2})} + \frac{K_2^2 Y_{rc3}}{K_1 Y_{rc3} + K_3^2} + Y_{rc2}} \tag{17}$$

$$v_{\rm out3} = \frac{K_3 v_{\rm in} - K_2 K_3 v_{\rm out2}}{K_1 Y_{rc3} + K_3^2}. \tag{18}$$

Derivations of (17) and (18), and definition of the parameters are given in Appendixes C and D

$$V_L = \frac{R_L}{R_L + r_{\rm rect2}} \left(\frac{2}{\pi} V_{\rm out2,pk} - 2V_D \right) \tag{19}$$

$$i_{\rm in} = \frac{v_{\rm in} - K_2 v_{\rm out2} - K_3 v_{\rm out3}}{K_1} \tag{20}$$

where $V_{\rm out2,pk}$ is the amplitude of $v_{\rm out2}$.

3) *Mode 3—Only orthogonal winding transferring energy to the load:* This mode occurs when the transmitting coil and the parallel winding are significantly misaligned. Fig. 10(d) shows the equivalent circuit model. $v_{\rm out2}$, $v_{\rm out3}$, and V_L can be expressed as

$$v_{\rm out2} = \frac{K_2 v_{\rm in} - K_2 K_3 v_{\rm out3}}{K_1 Y_{rc2} + K_2^2} \tag{21}$$

$$v_{\rm out3} \approx \frac{\frac{K_3 Y_{rc2}}{K_1 Y_{rc2} + K_2^2} v_{\rm in} + \frac{8}{\pi (R_L + r_{\rm rect3})} V_D}{\frac{8}{\pi^2 (R_L + r_{\rm rect3})} + \frac{K_3^2 Y_{rc2}}{K_1 Y_{rc2} + K_2^2} + Y_{rc3}} \tag{22}$$

$$V_L = \frac{R_L}{R_L + r_{\rm rect3}} \left(\frac{2}{\pi} V_{\rm out3,pk} - 2V_D \right) \tag{23}$$

where $V_{\rm out3,pk}$ is the amplitude of $v_{\rm out3}$.

The input current $i_{\rm in}$ in this mode has the same expression as (20).

D. Boundary Conditions for Determining the Operating Modes

The operating mode of the proposed circuit is determined by the ratio between k_{12} and k_{13}, where k_{12} is the coupling coefficient between the transmitting coil and the parallel winding, and k_{13} is the coupling coefficient between the transmitting coil and the orthogonal winding.

In the Mode 1 operation

$$i_{\text{out}2} > 0 \quad \text{and} \quad i_{\text{out}3} > 0. \tag{24}$$

In the Mode 2 operation

$$i_{\text{out}2} > 0 \quad \text{and} \quad i_{\text{out}3} = 0. \tag{25}$$

In the Mode 3 operation

$$i_{\text{out}2} = 0 \quad \text{and} \quad i_{\text{out}3} > 0. \tag{26}$$

The boundary between Modes 1 and 2 is determined by the conditions

$$v_{\text{out}2} = v_{\text{out}3} \tag{27}$$

and

$$i_{\text{out}3} = 0. \tag{28}$$

Define

$$\Psi = \frac{k_{12}}{k_{13}}. \tag{29}$$

Based on (17) and (18), the circuit will be in Mode 2 operation if

$$\Psi \geq (\Psi_{M1-M2})^{-1} \tag{30}$$

where $\Psi_{M1-M2} = \frac{1}{Q_3\left[\frac{1}{Q_2} - \frac{8r_2}{\pi^2 R_L}(1+Q_2)\right]}\sqrt{\frac{L_2}{L_3}}$.

The expression and derivation of Ψ_{M1-M2} are given in Appendix E.

Similarly, the boundary between Modes 1 and 3 is determined by the conditions

$$v_{\text{out}2} = v_{\text{out}3} \tag{31}$$

and

$$i_{\text{out}2} = 0. \tag{32}$$

Based on (21) and (22), the circuit will be in Mode 3 operation if

$$\Psi \leq \Psi_{M1-M3} \tag{33}$$

where $\Psi_{M1-M3} = \frac{1}{Q_2\left[\frac{1}{Q_3} - \frac{8r_3}{\pi^2 R_L}(1+Q_3)\right]}\sqrt{\frac{L_3}{L_2}}$.

Derivation of Ψ_{M1-M3} is similar to the derivation of Ψ_{M1-M2} in Appendix E, under the condition that $v_{\text{out}2} = v_{\text{out}3}$ and $i_{\text{out}2} = 0$.

Fig. 11 shows the boundaries for the three modes on the $k_{12}-k_{13}$ plane with three different turns-ratios between the parallel and orthogonal windings. They are 12:6, 12:12, and 12:24. Thus, both windings are concurrently energized within a wide range of coupling coefficient (i.e., in Mode 1 operation). The regions covered by Modes 2 and 3 is determined by the values of L_2 and L_3. When $L_3 > L_2$, the area covered by Mode 3 is more than that covered by Mode 2, and vice versa. For example, as shown in Fig. 11(a), $N_2 : N_3 = 12 : 26$, the area covered by Mode 2 is larger than the area covered by Mode 3. Conversely, as shown in Fig. 11(c), $N_2 : N_3 = 12 : 24$, the area covered by Mode 3 is larger than that by Mode 2.

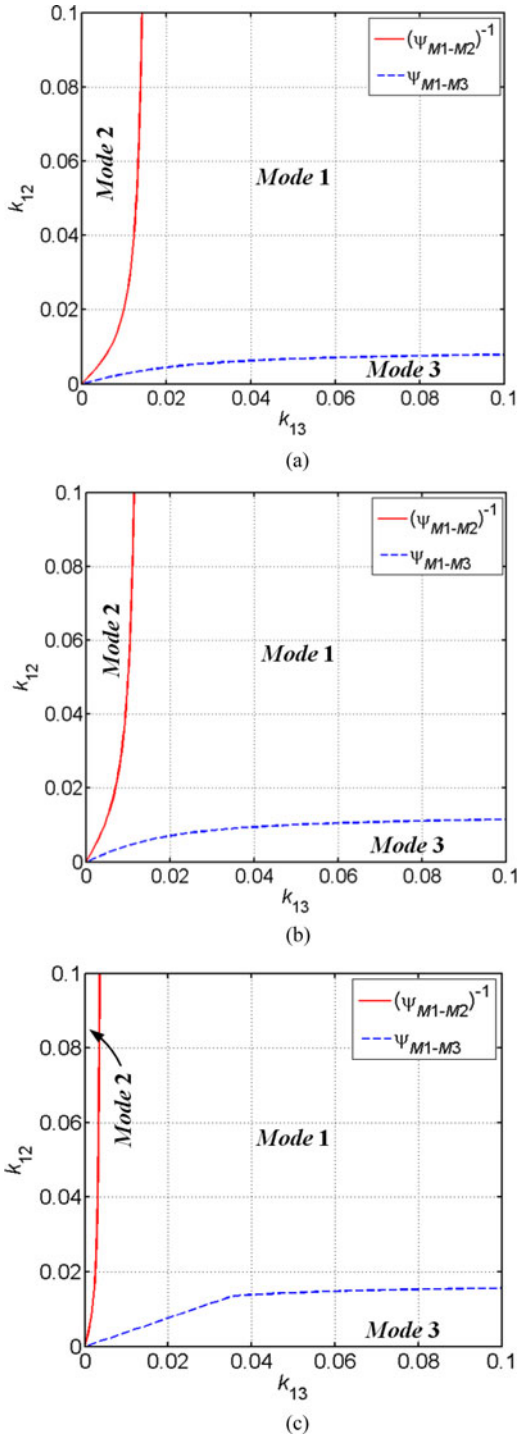

Fig. 11. Mode of operation on the $k_{12}-k_{13}$ plane. (a) $N_2 : N_3 = 12 : 6$. (b) $N_2 : N_3 = 12 : 12$. (c) $N_2 : N_3 = 12 : 24$.

V. Power Transfer Efficiency

The power transfer efficiencies of the parallel coils and the proposed structure are studied and compared. As shown in Fig. 1, the power transfer efficiency η is calculated by

$$\eta = \frac{P_{\text{out}}}{P_{\text{in}}} = \frac{V_L^2/R_L}{\text{Re}[v_{\text{in}} i_{\text{in}} *]} \tag{34}$$

where P_{out} is the output power to the load R_L, P_{in} is the input power to the transmitting coil, i_n^* is the conjugate of i_{in}, and $\text{Re}[v_{\text{in}} i_{\text{in}} *]$ means the real part.

Based on the dimensions, positions, orientations, and number of turns of the coils, the mutual inductances M_{12} and M_{13} are obtained by using (3). The coupling coefficients k_{12} and k_{13} are determined by using the equations

$$k_{12} = \frac{M_{12}}{\sqrt{L_1 L_2}} \tag{35}$$

and

$$k_{13} = \frac{M_{13}}{\sqrt{L_1 L_3}}. \tag{36}$$

The mode of operation is located by using the values of k_{12} and k_{13} on the $k_{12}-k_{13}$ plane in Fig. 11. Then, the optimal load resistance $R_{L,\text{optimal}}$ is determined by using an iterative method. Fig. 12 shows the flowchart. The steps are described as follows:

1) choose the magnitudes of the lateral misalignment Δ and angular misalignment θ;
2) calculate M_{12} and M_{13} with (3), and determine the corresponding values of k_{12} and k_{13} with (35) and (36), respectively;
3) select an initial value of R_L, e.g., 100 Ω, and set $n = 1$;
4) calculate Ψ with (29);
5) calculate Ψ_{M1-M2} and Ψ_{M1-M3} with (30) and (33), respectively;
6) determine the mode of operation, based on the criteria given in Section IV-D;
7) calculate the values of V_L and i_{in} with the required set of equations, (11)–(16) for Mode 1, (17)–(20) for Mode 2, and (20)–(23) for Mode 3;
8) calculate $\eta\,(n)$ with (34) and compare it with $\eta(n-1)$;
9) terminate the iteration with $R_{L,\text{optimal}} = R_L(n)$ for the efficiency η at the considered misalignment if $|\eta(n) - \eta(n-1)| < \varepsilon_T$, and start from Step 1 with a new misalignment;
10) if not, increase the value R_L by ΔR_L, increment n, and repeat from Step 5.

Fig. 13(a) shows the 3-D surface of the power transfer efficiency versus different combinations of Δ and θ of classical parallel coils. Fig. 13(b) shows the 2-D contour graph of Fig. 13(a). Fig. 13(c) and (d) shows the power transfer efficiency of the proposed coil structure with the windings having the turns ratio of $N_2 : N_3 = 12 : 24$. The physical dimensions and electrical parameters of the transmitting coil and receiving coil are given in Tables I and II. As shown in Fig. 13(a), the efficiency surface of the parallel coils is like a "rugby ball." The rate of reduction of the efficiency versus lateral or angular misalignment becomes more severe when the efficiency is in the range of 30%, since the contour lines start getting closer from this range. The minimum efficiency is 0%, where the two coils are significantly misaligned. If the minimum efficiency considered is 30%, the maximum allowable lateral misalignment Δ ranges from -30% to $+30\%$ and angular misalignment θ ranges from $-35°$ to $+35°$. Such zone is shaded in Fig. 13(b).

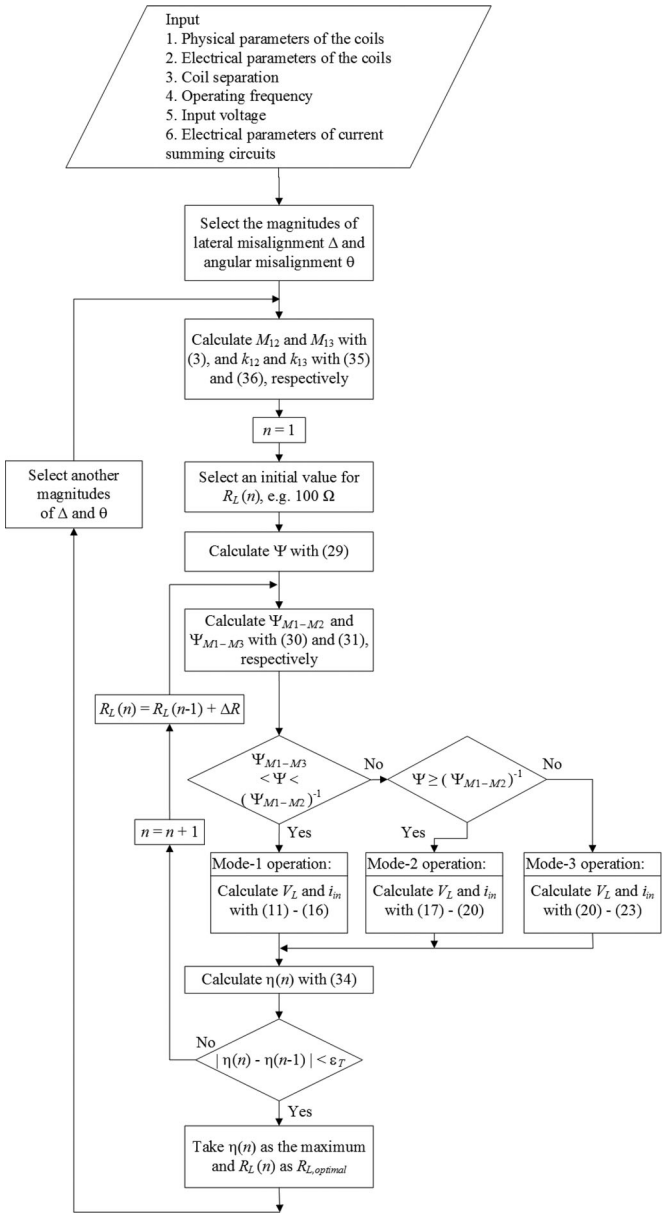

Fig. 12. Flowchart for calculating $R_{L,\text{optimal}}$ and η.

The efficiency surface of the proposed structure shown in Fig. 13(c) is more uniform and no abrupt efficiency drop is observed. Again, if the minimum efficiency of 30% is needed, the maximum allowable lateral misalignment Δ ranges from -45% to $+45\%$. The efficiency is always higher than 30% over the range of the angular misalignment. Such zone is shaded in Fig. 13(d). Thus, the misalignment tolerance of the proposed structure is better than the parallel coils.

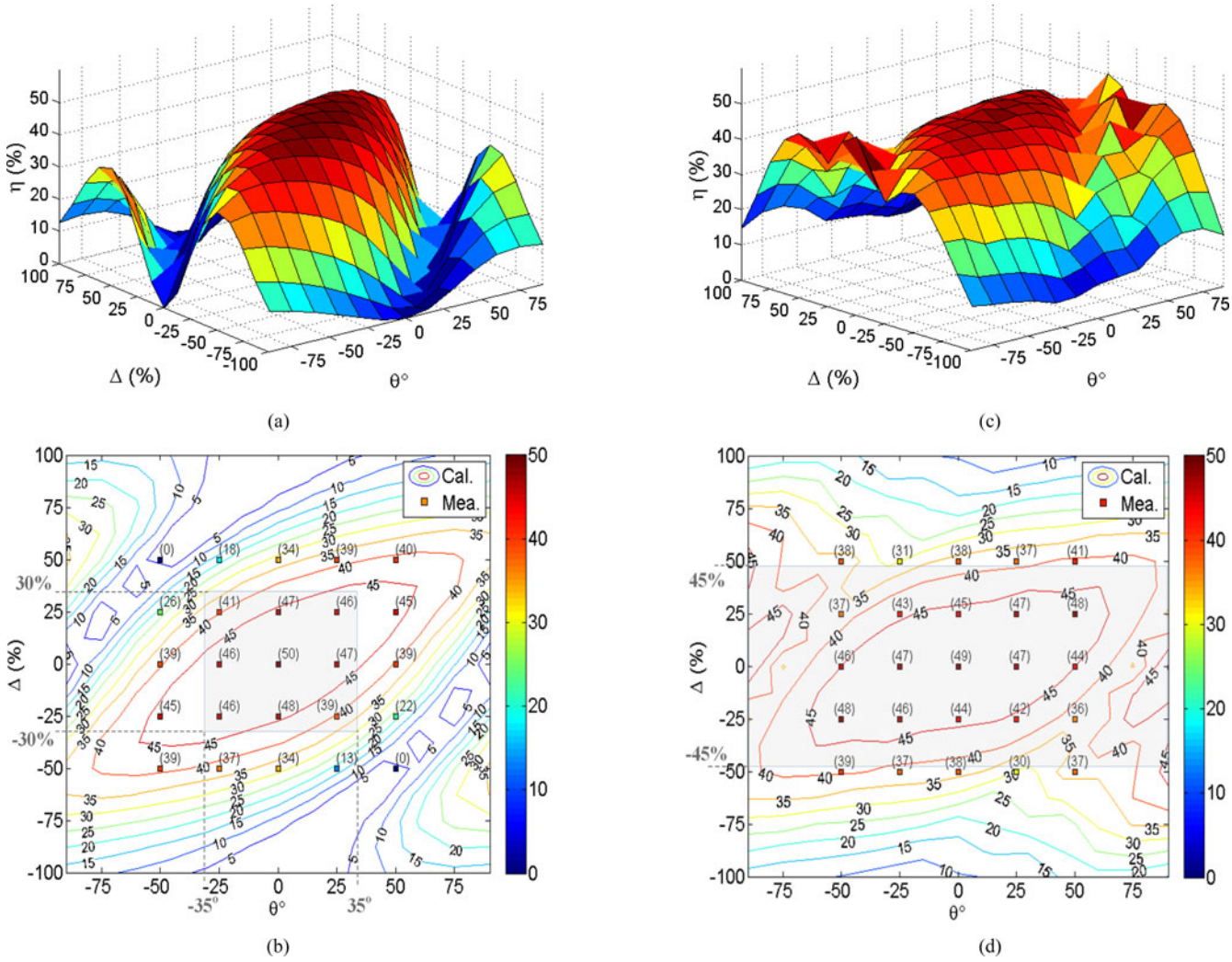

Fig. 13. Power transfer efficiency under both lateral and angular misalignments. (a) Three-dimensional efficiency surface of parallel coils. (b) Two-dimensional contour graph of (a). (c) Three-dimensional efficiency surface of the proposed structure. (d) Two-dimensional contour graph of (c).

VI. Experimental Verifications

The performances of the parallel coils and the proposed structure are studied and compared on a testing setup shown in Fig. 14. Such setup allows altering and measuring the degree of lateral and angular misalignments. The parameters of the 16-turn transmitting coil are given in Table I. Three sets of receiving coils, including the classical parallel coil with 12 turns, proposed T-shaped structure with 12 turns in the parallel winding and six turns in the orthogonal winding, and another T-shaped structure with 12 turns in the parallel winding and 24 turns in the orthogonal winding, are fabricated. The physical dimensions and electrical parameters of the coils are given in Table II. They are measured by Agilent Impedance Analyzer 4294A. The components used in the summing circuit are given in Table III. The transmitting coil is driven by an RF amplifier, Amplifier Research 75A250A. The operating frequency is 2.2 MHz, which is typically used in retinal implant [32]. The value of the load resistance is determined by the procedure depicted in the flowchart shown in Fig. 12. It ensures maximum efficiency in the power transfer from the transmitting coil to the load.

The load voltage is observed by using a voltage probe (Model no. Tektronix P6139B) on the oscilloscope (Model no. Tektronix TDS3032). The input current is observed by using a current probe (Model no. Tektronix TCP202) on the same oscilloscope and the time delay (17 ns) for the current probe signal is taken into account. The input power is obtained by averaging the product of the input voltage $v_{\rm in}$ and the input current $i_{\rm in}$, where the time series of the voltage and current waveforms are first captured on the oscilloscope.

Fig. 6 shows the measured percentage variation of the mutual inductance between the transmitting and the parallel receiving coils under lateral and angular misalignment. Fig. 8 shows the measured percentage variation of M_{12} and M_{13} of the proposal coil with the turns ratio of $N_2 : N_3 = 12 : 24$ under lateral and angular misalignments.

With the parallel and orthogonal windings in the receiving coil connected as in Fig. 10(a), Fig. 15(a) shows the measured

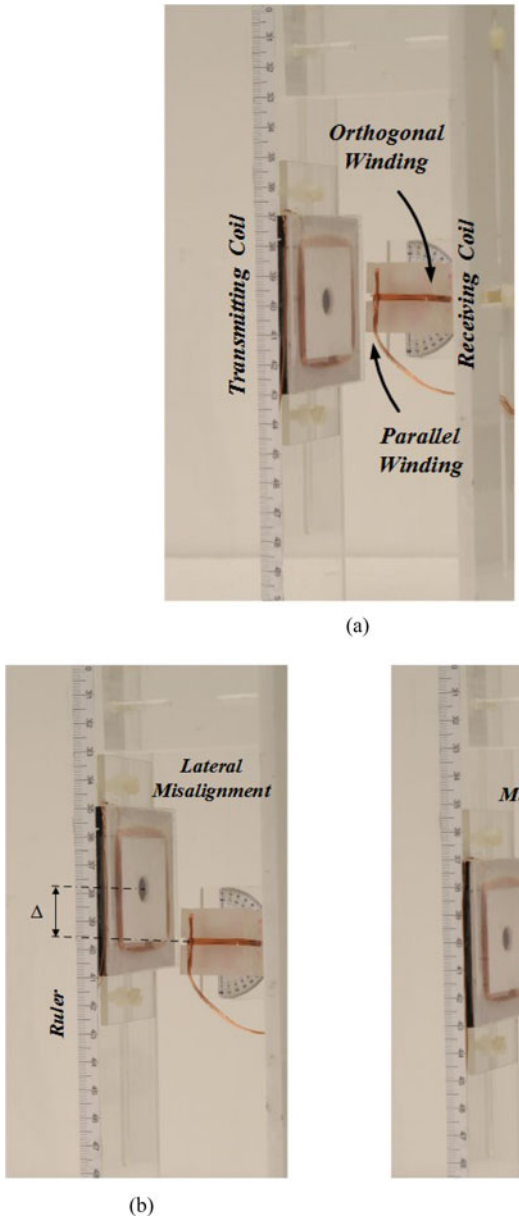

Fig. 14. Experimental setup. (a) Aligned condition. (b) Lateral misalignment. (c) Angular misalignment.

transfer efficiency of the three testing receiving coils under lateral misalignment with $\theta = 0$. Fig. 15(b) shows the measured results under angular misalignment with $\Delta = 0\%$. The ranges of the operating modes are marked on the graphs.

Fig. 13(b) shows the measured efficiencies with the parallel receiving coil oriented at 25 combinations of lateral and angular misalignments. The lateral alignment is ranged from -50% to $+50\%$, while the angular misalignment is ranged from $-50°$ to $+50°$. Similarly, Fig. 13(d) shows the measured efficiencies with the T-shaped structure with the turns ratio of $N_2 : N_3 = 12 : 24$ at the same orientations measured in Fig. 13(b). The theoretical predictions shown on the contours are close to the experimental results.

TABLE III
COMPONENT VALUES OF THE OUTPUT CURRENT SUMMING CIRCUIT

$v_{\text{in,peak}}$	$D_{2i} \sim D_{3i}*$	L_{rect2} and L_{rect3}	r_{rect2} and r_{rect3}
5 V	1N4148	0.92 mH	15.0 Ω

$^*i = 1$–4.

A power loss audit of three cases in the three modes has been conducted. The results are shown in Table IV. It was found that the major loss is in the winding resistances. Thus, if the operating frequency is increased, the power loss in the windings will increase as the ac resistance of the windings will increase, due to the skin effect and proximity effects [28].

Fig. 16 shows the waveforms of i_{out2}, i_{out3}, and I_L under different combinations of lateral and angular misalignments with $i_{\text{out2}} : i_{\text{out3}} = 6 : 1,\ 1 : 1$, and $1 : 6$. I_L is found to be the sum of the rectified value of i_{out2} and i_{out3} in all cases, confirming the current summing technique. The waveforms of i_{out2} and i_{out3} are near square waveform, confirming the modeling of the corresponding current sources given in Section IV.

VII. OBSERVATIONS AND DISCUSSIONS

Based on the theoretical analysis and experimental results, some observations are made and future investigations are suggested.

1) Based on Figs. 13 and 15, it is confirmed that the orthogonal winding can effectively improve the transfer efficiency under coil misalignment. Thus, more orthogonal windings can be added to form complex loosely coupled winding structures. For example, a second orthogonal winding can be added onto the receiving coil. Then, the structure can tackle misalignment of a higher dimension. As the analysis method discussed in this paper starts from the basic principle, similar analysis can be adopted for studying the structure with the second orthogonal winding.
2) Compared Fig. 13(a) with Fig. 13(c), the overall transfer efficiency of the proposed structure will never go to zero within the considered range of the misalignments, because either one or both of the windings will have coupling with the transmitting coil. Conversely, the classical parallel coil could have zero efficiency.
3) The canonical transformer model presented in Section IV gives an alternative circuit model to study the coupling phenomenon of windings. Experimental results confirm the validity of the circuit model. Since the output winding is modeled as a current source in parallel with an inductance, it is suitable for modeling complex structures with several parallel windings.
4) The current summing technique with the added output inductors L_{rect2} and L_{rect3}, shown in Fig. 10(a), can keep both windings energized to deliver power to the load. As shown in Fig. 11, except under extreme low values of the coupling coefficients k_{12} and k_{13}, the entire circuit will operated in Mode 1, that is, both windings transfer energy to the load.

TABLE IV
POWER LOSS AUDIT IN THE THREE MODES

Mode	P_{in} (mW)	P_{out} (mW)	Loss of r_1^* (%)	Loss of r_2^* (%)	Loss of r_3^* (%)	Loss of the diode bridges* (%)	Loss of r_{rect2}^* and r_{rect3}^* (%)
I	896	330	41.11	15.38	3.11	3.23	0.34
II	619	304	27.51	17.95	0.00	4.56	0.87
III	1448	173	75.46	2.31	9.61	0.66	0.02

*The losses are all normalized by the input power P_{in}.

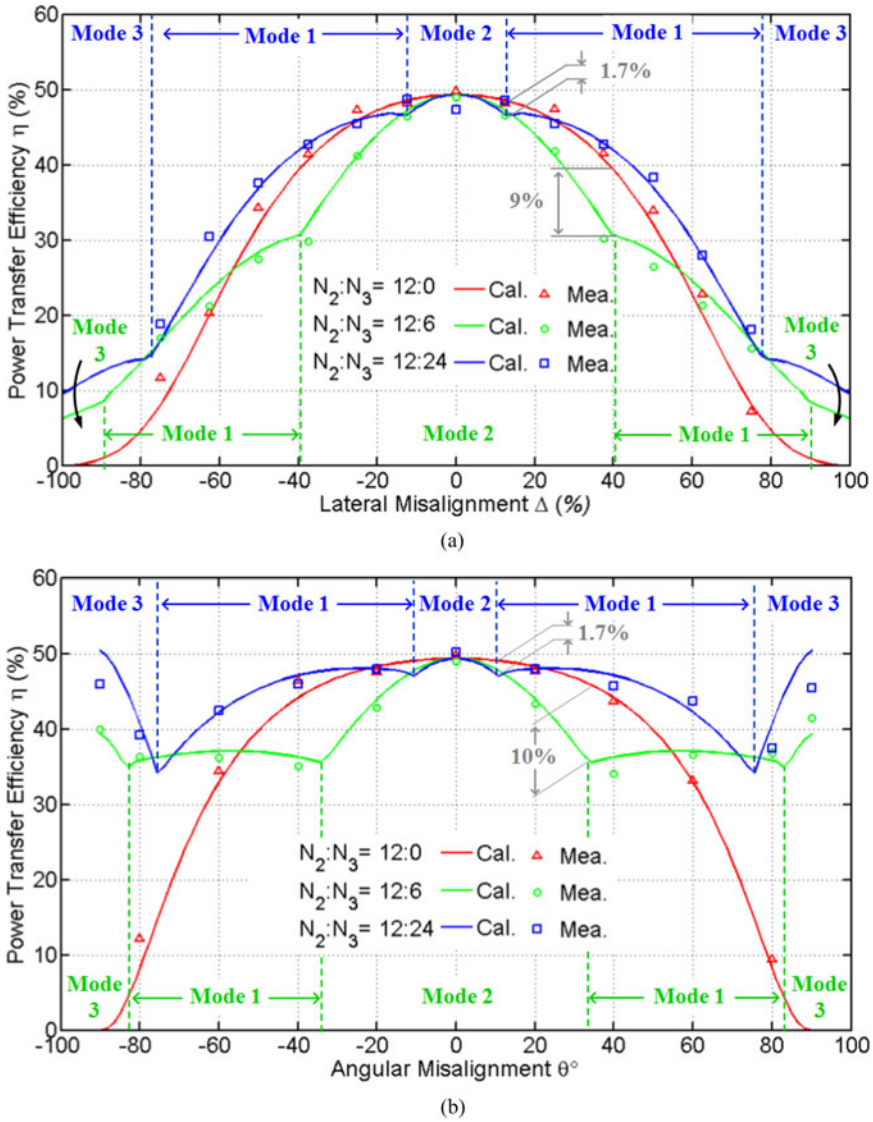

Fig. 15. Measured power transfer efficiency of different coil sets with parallel and orthogonal windings under lateral and angular misalignments. (a) Efficiency curves under lateral misalignment. (b) Efficiency curves under angular misalignment.

5) As shown in Fig. 15, when the circuit is in Mode 2 operation, the transfer efficiency of the proposed structure is lower than with just the parallel coil. As shown in Fig. 10(c), it is mainly because a small amount of energy is dissipated in the orthogonal winding. In order to reduce the difference, the range of Mode 2 operation can be reduced by increasing the number of turns of the orthogonal winding. As shown in Fig. 15 (from green line to blue line), with the number of turns in the orthogonal winding increasing from 6 to 24, the range of the Mode 2 operation is reduced. As exemplified in Fig. 15, with the number of turns increased from 6 turns to 24 turns, the difference in the transfer efficiency is reduced from 9% to 1.7% in the lateral misalignment and from 10% to 1.7% in the angular misalignment. Such phenomenon can be explained by considering that the impedance of the orthogonal winding is increased. Thus, the current through the winding, and thus its power loss, are reduced.

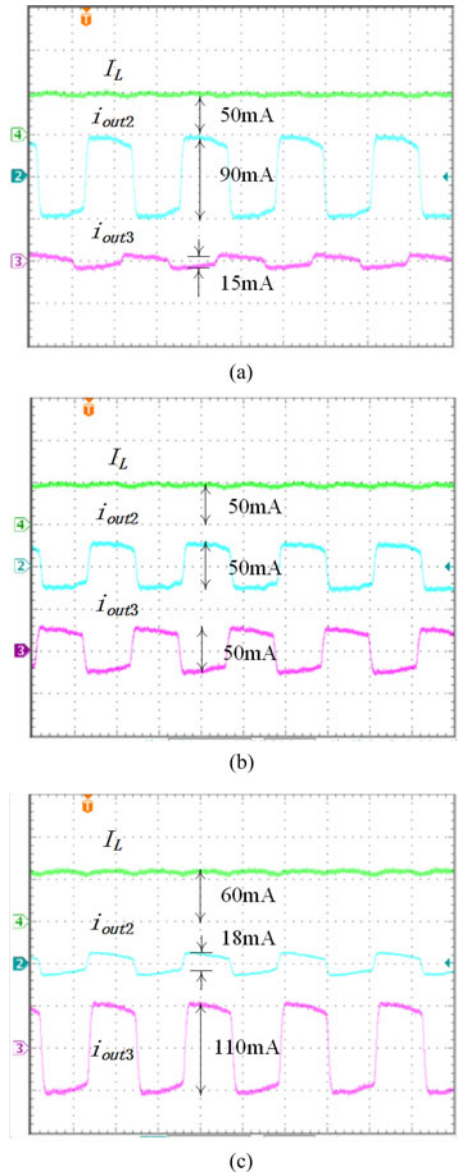

Fig. 16. Waveforms of $i_{\rm out2}$, $i_{\rm out3}$, and I_L under different misalignments [Ch2: $i_{\rm out2}$, Ch3: $i_{\rm out3}$, Ch4: I_L (50 mA/div)] (Timebase: 200 ns/div). (a) $i_{\rm out2} : i_{\rm out3} = 6 : 1$. (b) $i_{\rm out2} : i_{\rm out3} = 1 : 1$. (c) $i_{\rm out2} : i_{\rm out3} = 1 : 6$.

However, the number of turns cannot be continually increased, as there is a maximum achievable efficiency, similar to the characteristics of the parallel coil shown in Fig. 2. The difference of 1.7% is acceptable in practice, as there is a significant improvement in the efficiency under coil misalignment.

6) The efficiency drop issue discussed in item (5) may be solved by using a circuit to disable the orthogonal winding upon Mode 2 operation, such as the method discussed in [26]. However, special consideration should be given to the increase of the circuit complexity.
7) As shown in Fig. 15, when the circuit is in Mode 3 operation, the orthogonal winding takes up the main energy transfer. Since the coupling of the transmitting coil and the orthogonal winding is good, the transfer efficiency will increase abruptly.

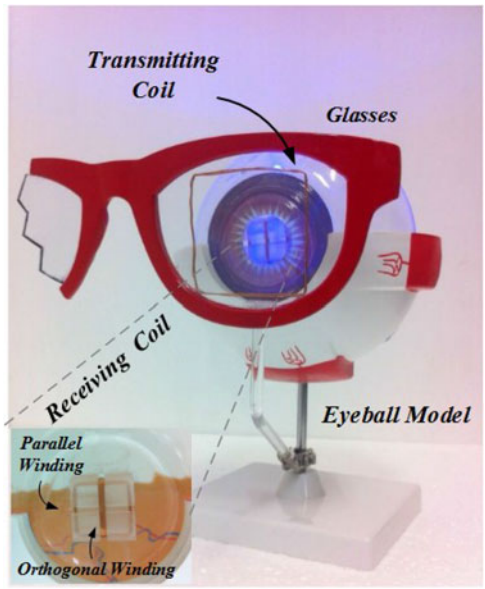

Fig. 17. Illustration of the application of the proposed winding structure.

8) It is understandable that the orthogonal winding can be placed in the transmitting coil and the receiving coil is a parallel winding. Driving of the transmitting coil can be similar to the one described in [8] and [24]. More complex winding structures can also be deduced.
9) Fig. 17 shows a model illustrating how the proposed structure can be placed inside an eyeball for a visual prosthesis [33], [34]. Electric power can be transmitted from the glasses. Complex structures can also be deduced for applications, like capsular endoscope, requiring dealing with high-dimension misalignment. Further investigations can be emphasized on the relationships among the operating frequency, coil size, and space constraint of the application.

VIII. Conclusion

A comprehensive investigation into the use of an orthogonal winding in loosely coupled link for enhancing transfer efficiency under coil misalignment has been presented. Both theoretical and experimental results confirm that the power transfer efficiency under coil misalignment can be effectively increased with the added orthogonal winding. A canonical transformer model has been derived and applied to study the proposed structure. Moreover, a current summing technique has been proposed to energize the parallel and orthogonal windings over a wide range of misalignments. The concept has been verified on a test bed.

Appendix A
Expressions of the Parameters in (2)

$$BD = R_1, BC = R_2, AC = R_3, AD = R_4, \cos\varepsilon = \frac{\alpha^2}{2lm},$$
$$\alpha^2 = R_4^2 - R_3^2 + R_2^2 - R_1^2,$$

$$d^2 = R_3^2 - \mu^2 - \nu^2 + 2\mu\nu\cos\varepsilon,$$
$$\mu = \frac{l[2m^2(R_2^2 - R_3^2 - l^2) + \alpha^2(R_4^2 - R_3^2 - m^2)]}{4l^2m^2 - \alpha^4},$$
$$\nu = \frac{m[2l^2(R_4^2 - R_3^2 - m^2) + \alpha^2(R_2^2 - R_3^2 - l^2)]}{4l^2m^2 - \alpha^4}$$

and

$$\Omega = \tan^{-1}\left[\frac{d^2\cos\varepsilon + (\mu + l)(\nu + m)\sin^2\varepsilon}{d\,R_1\sin\varepsilon}\right] - \tan^{-1}\left[\frac{d^2\cos\varepsilon + (\mu + l)\,\nu\sin^2\varepsilon}{d\,R_2\sin\varepsilon}\right] + \tan^{-1}\left[\frac{d^2\cos\varepsilon + \mu\,\nu\sin^2\varepsilon}{d\,R_3\sin\varepsilon}\right] - \tan^{-1}\left[\frac{d^2\cos\varepsilon + \mu(\nu + m)\sin^2\varepsilon}{d\,R_4\sin\varepsilon}\right].$$

Appendix B
Derivation of (9) and (10)

Based on Fig. 9(a), the ideal transformer has the primary-side voltage v_{1T} and current i_{1T}, and the secondary-side voltage v_{2T} and current i_{2T}. Thus,

$$V_{1T}(s) = n_{12}V_{2T}(s) \tag{B1}$$
$$V_{1T}(s) = sn_{12}M[I_1(s) - I_{1T}(s)] \tag{B2}$$
$$V_{2T}(s) = \left[r_2 + s\left(L_2 - \frac{M}{n_{12}}\right)\right]I_{2T}(s) + V_2(s) \tag{B3}$$

$$sM\,[I_1(s) - I_{1T}(s)] = \left[r_2 + s\left(L_2 - \frac{M}{n_{12}}\right)\right]I_{2T}(s) + V_2(s)$$
$$I_{1T}(s) = \frac{I_{2T}(s)}{n_{12}}$$
$$I_2(s) = \frac{sM}{r_2 + sL_2}I_1(s) - \frac{1}{r_2 + s\left(L_2 - \frac{M}{n_{12}}\right) + s\frac{M}{n_{12}}}V_2(s). \tag{B4}$$

By substituting (B6) into (B3) and (B1)

$$V_{1T}(s) = \frac{s\frac{M}{n_{12}}\left[r_2 + s\left(L_2 - \frac{M}{n_{12}}\right)\right]}{r_2 + s\left(L_2 - \frac{M}{n_{12}}\right) + s\frac{M}{n_{12}}}n_{12}^2I_1(s) + \frac{s\frac{M}{n_{12}}}{r_2 + s\left(L_2 - \frac{M}{n_{12}}\right) + s\frac{M}{n_{12}}}n_{12}V_2(s) \tag{B7}$$

$$V_1(s) = \left\{r_1 + s(L_1 - n_{12}M) + \frac{sn_{12}M\left[n_{12}^2r_2 + sn_{12}^2\left(L_2 - \frac{M}{n_{12}}\right)\right]}{n_{12}^2r_2 + sn_{12}^2\left(L_2 - \frac{M}{n_{12}}\right) + sn_{12}M}\right\}I_1(s) + \frac{s\frac{M}{n_{12}}}{r_2 + s\left(L_2 - \frac{M}{n_{12}}\right) + s\frac{M}{n_{12}}}n_{12}V_2(s). \tag{B8, B9}$$

Appendix C
Derivations of (11) and (12)

Let

$$K_1 = r_1 + j\omega L_1 + \frac{1}{j\omega C_1} - \frac{(j\omega M_{12})^2}{r_2 + j\omega L_2} - \frac{(j\omega M_{13})^2}{r_3 + j\omega L_3}$$
$$K_2 = \frac{j\omega M_{12}}{r_2 + j\omega L_2}$$
$$K_3 = \frac{j\omega M_{13}}{r_3 + j\omega L_3}$$
$$n_{12}v_{d2} = K_2v_{\text{out}2},\ \ n_{13}v_{d3} = K_3v_{\text{out}3} \tag{C1}$$
$$i_{\text{in}} = \frac{v_{\text{in}} - K_2v_{\text{out}2} - K_3v_{\text{out}3}}{K_1} \tag{C2}$$
$$n_{12}i_{d2} = K_2i_{\text{in}}, n_{13}i_{d3} = K_3i_{\text{in}}. \tag{C3}$$

The admittances of the receiving parallel resonant circuits, Y_{rc2} and Y_{rc3}, are

$$Y_{rc2} = \frac{1 + j\omega C_2(r_2 + j\omega L_2)}{r_2 + j\omega L_2}$$
$$Y_{rc3} = \frac{1 + j\omega C_3(r_3 + j\omega L_3)}{r_3 + j\omega L_3}.$$

When the inductance of $L_{\text{rect}2}$ and $L_{\text{rect}3}$ are large enough, $I_{\text{rect}2}$ and $I_{\text{rect}3}$ can be considered as constant dc current, so the current input to the rectifier $i_{\text{out}2}$ and $i_{\text{out}3}$ should be in form of square wave. The fundamental current components are

$$\tilde{i}_{\text{out}2} = n_{12}i_{d2} - Y_{rc2}v_{\text{out}2},\ \tilde{i}_{\text{out}3} = n_{13}i_{d3} - Y_{rc3}v_{\text{out}3} \tag{C4}$$

$$|i_{\text{out}2}| = \frac{\pi}{4}\tilde{i}_{\text{out}2,\text{peak}},\ |i_{\text{out}3}| = \frac{\pi}{4}\tilde{i}_{\text{out}3,\text{peak}}. \tag{C5}$$

By combining (C1)–(C5)

$$I_{\text{rect}2} = |i_{\text{out}2}| = \frac{\pi}{4}\left[\frac{K_2}{K_1}(v_{\text{in}} - K_2v_{\text{out}2} - K_3v_{\text{out}3}) - Y_{rc2}v_{\text{out}2}\right]_{,\text{peak}} \tag{C6}$$

$$I_{\text{rect}3} = |i_{\text{out}3}| = \frac{\pi}{4}\left[\frac{K_3}{K_1}(v_{\text{in}} - K_2v_{\text{out}2} - K_3v_{\text{out}3}) - Y_{rc3}v_{\text{out}3}\right]_{,\text{peak}} \tag{C7}$$

$$\overline{V}_{\text{rect}2} = \frac{2}{\pi}v_{\text{out}2,\text{peak}} - 2V_{D2},\ \overline{V}_{\text{rect}3} = \frac{2}{\pi}v_{\text{out}3,\text{peak}} - 2V_{D3} \tag{C8}$$

$$V_L = \overline{V}_{\text{rect}2} - I_{\text{rect}2}r_{\text{rect}2},\ V_L = \overline{V}_{\text{rect}3} - I_{\text{rect}3}r_{\text{rect}3}. \tag{C9}$$

By combining (C6)–(C9)

$$\frac{2}{\pi}v_{\text{out2,peak}} - 2V_{D2} - \frac{\pi}{4}\tilde{i}_{\text{out2,peak}}r_{\text{rect2}} = \frac{2}{\pi}v_{\text{out3,peak}} - 2V_{D3} - \frac{\pi}{4}\tilde{i}_{\text{out3,peak}}r_{\text{rect3}}. \quad \text{(C10)}$$

When ωL_{rect2} and ωL_{rect3} are larger than the load resistance R_L, v_{out2} and v_{out3} are in the same phase φ

$$\frac{2}{\pi}v_{\text{out2}} - 2V_{D2}\angle\phi - \frac{\pi}{4}\tilde{i}_{\text{out2}}r_{\text{rect2}} = \frac{2}{\pi}v_{\text{out3}} - 2V_{D3}\angle\phi - \frac{\pi}{4}\tilde{i}_{\text{out3}}r_{\text{rect3}}$$

$$v_{\text{out3}} = \frac{H_2 v_{\text{out2}} - H_1 v_{\text{in}} - 2(V_{D2} - V_{D3})\angle\phi}{H_3} \quad \text{(C11)}$$

where

$$H_1 = \frac{\pi}{4}\frac{(K_2 r_{\text{rect2}} - K_3 r_{\text{rect3}})}{K_1}$$

$$H_2 = \frac{2}{\pi} + \frac{\pi}{4}\left[\frac{K_2(K_2 r_{\text{rect2}} - K_3 r_{\text{rect3}})}{K_1} + Y_{rc2} r_{\text{rect2}}\right]$$

$$H_3 = \frac{2}{\pi} + \frac{\pi}{4}\left[\frac{K_3(K_3 r_{\text{rect3}} - K_2 r_{\text{rect2}})}{K_1} + Y_{rc3} r_{\text{rect3}}\right]$$

$$V_L = \bar{V}_{\text{rect2}} - I_{\text{rect2}} r_{\text{rect2}} = (I_{\text{rect2}} + I_{\text{rect3}})R_L. \quad \text{(C12)}$$

By substituting (C5) to (C8) into (C12), (C13) as shown at the bottom of the page, where $H_4 = \frac{1}{K_1}\left[K_2\left(1 + \frac{r_{\text{rect2}}}{R_L}\right) + K_3\right]$. Since C_1, C_2, and C_3 resonate with the respective winding self-inductance, the phase angle of the output voltages φ is near zero.

Appendix D
Derivations of (17) and (18)

$$n_{13} i_{d3} = Y_{rc3} v_{\text{out3}} \quad \text{(D1)}$$

$$n_{13} i_{d3} = K_3\left(\frac{v_{\text{in}} - K_2 v_{\text{out2}} - K_3 v_{\text{out3}}}{K_1}\right). \quad \text{(D2)}$$

By combining (D1) and (D2)

$$v_{\text{out3}} = \frac{K_3 v_{\text{in}} - K_2 K_3 v_{\text{out2}}}{K_1 Y_{rc3} + K_3^2} \quad \text{(D3)}$$

$$I_{\text{rect2}} = |i_{\text{out2}}| = \frac{\pi}{4}\left[\frac{K_2}{K_1}(v_{\text{in}} - K_2 v_{\text{out2}} - K_3 v_{\text{out3}}) - Y_{rc2} v_{\text{out2}}\right]_{,\text{peak}}$$

$$V_L = \frac{2}{\pi}v_{\text{out2,peak}} - 2V_{D2} - I_{\text{rect2}} r_{\text{rect2}} = I_{\text{rect2}} R_L. \quad \text{(D5)}$$

By combining (D3) and (D5)

$$v_{\text{out2}} = \frac{\frac{K_2 Y_{rc3}}{K_1 Y_{rc3} + K_3^2} v_{\text{in}} + \frac{8}{\pi(R_L + r_{\text{rect2}})} V_{D2}\angle\phi}{\frac{8}{\pi^2(R_L + r_{\text{rect2}})} + \frac{K_2^2 Y_{rc3}}{K_1 Y_{rc3} + K_3^2} + Y_{rc2}}. \quad \text{(D6)}$$

Since C_1 and C_2 resonate with the respective winding self-inductance, the phase angle of v_{out2} φ can be considered as zero.

Appendix E
Derivation of (30)

For the sake of simplicity, V_{D2}, V_{D3}, r_{rect2}, and r_{rect3} are neglected. Then

$$v_{\text{out2}} = v_{\text{out3}} = v_{\text{out}} \quad \text{(E1)}$$

$$i_{\text{out3}} = 0 \quad \text{(E2)}$$

$$n_{12} i_{d2} = \frac{K_2}{K_1}\left[v_{\text{in}} - (K_2 + K_3)v_{\text{out}}\right],$$

$$n_{13} i_{d3} = \frac{K_3}{K_1}\left[v_{\text{in}} - (K_2 + K_3)v_{\text{out}}\right] \quad \text{(E3)}$$

$$I_{\text{rect2}} = |i_{\text{out2}}| = \frac{\pi}{4}\left[n_{12} i_{d2} - Y_{rc2} v_{\text{out}}\right]_{,\text{peak}} \quad \text{(E4)}$$

$$V_L = \frac{2}{\pi}v_{\text{out,peak}} = I_{\text{rect2}} R_L. \quad \text{(E5)}$$

By combining (E3)–(E5)

$$v_{\text{out}} = \frac{\frac{K_2}{K_1} v_{\text{in}}}{\frac{8}{\pi^2 R_L} + \frac{K_2(K_2 + K_3)}{K_1} + Y_{rc2}} \quad \text{(E6)}$$

$$n_{13} i_{d3} = Y_{rc3} v_{\text{out}}. \quad \text{(E7)}$$

By combining (E3)–(E7)

$$v_{\text{out}} = \frac{\frac{K_3}{K_1} v_{\text{in}}}{\frac{K_3(K_2 + K_3)}{K_1} + Y_{rc3}}. \quad \text{(E8)}$$

By substituting (E6) into (E8)

$$\frac{\frac{K_2}{K_1} v_{\text{in}}}{\frac{8}{\pi^2 R_L} + \frac{K_2(K_2 + K_3)}{K_1} + Y_{rc2}} = \frac{\frac{K_3}{K_1} v_{\text{in}}}{\frac{K_3(K_2 + K_3)}{K_1} + Y_{rc3}}$$

$$\frac{2}{\pi}v_{\text{out2,peak}} - 2V_{D2} - \frac{\pi}{4}\tilde{i}_{\text{out2,peak}}r_{\text{rect2}} = \frac{\pi}{4}(\tilde{i}_{\text{out2,peak}} + \tilde{i}_{\text{out3,peak}})R_L$$

$$\frac{2}{\pi}v_{\text{out2}} - 2V_{D2}\angle\phi - \frac{\pi}{4}\tilde{i}_{\text{out2}}r_{\text{rect2}} = \frac{\pi}{4}(\tilde{i}_{\text{out2}} + \tilde{i}_{\text{out3}})R_L$$

$$v_{\text{out2}} = \frac{\left[H_4 + \frac{H_1}{H_3}(Y_{rc3} + K_3 H_4)\right] v_{\text{in}} + \frac{8}{\pi R_L} V_{D2}\angle\phi + \frac{2(Y_{rc3} + K_3 H_4)}{H_3}(V_{D2} - V_{D3})\angle\phi}{\frac{8}{\pi^2 R_L} + Y_{rc2}\left(1 + \frac{r_{\text{rect2}}}{R_L}\right) + Y_{rc3}\frac{H_2}{H_3} + \frac{(K_2 H_3 + K_3 H_2)H_4}{H_3}} \quad \text{(C13)}$$

$$\frac{K_3}{K_2} = \frac{Y_{rc3}}{Y_{rc2} + \frac{8}{\pi^2 R_L}}. \quad \text{(E9)}$$

By substituting K_2 and K_3 into (E9)

$$\frac{M_{13}}{M_{12}} = \frac{1}{Q_3\left[\frac{1}{Q_2} - \frac{8r_2}{\pi^2 R_L}(1+Q_2)\right]} \quad \text{(E10)}$$

where $Q_2 = \frac{j\omega L_2}{r_2}$ and $Q_3 = \frac{j\omega L_3}{r_3}$.

M_{12} and M_{13} can be expressed in term of their corresponding coupling coefficient k_{12} and k_{13}

$$M_{12} = k_{12}\sqrt{L_1 L_2} \text{ and } M_{13} = k_{13}\sqrt{L_1 L_3}. \quad \text{(E11)}$$

By combining (E10) and (E11)

$$\begin{aligned}\Psi_{M1-M2} &= \frac{k_{13}}{k_{12}}\Big|_{v_{\text{out}2}=v_{\text{out}3},\, i_{\text{out}3}=0} \\ &= \frac{M_{13}}{M_{12}}\sqrt{\frac{L_2}{L_3}}\Big|_{v_{\text{out}2}=v_{\text{out}3},\, i_{\text{out}3}=0} \\ &= \frac{1}{Q_3\left[\frac{1}{Q_2} - \frac{8\,r_2}{\pi^2 R_L}(1+Q_2)\right]}\sqrt{\frac{L_2}{L_3}}. \quad \text{(E12)}\end{aligned}$$

REFERENCES

[1] F. A. Spelman, "The past, present, and future of cochlear prostheses," *IEEE Eng. Med. Biol. Mag.*, vol. 18, no. 3, pp. 27–33, May/Jun. 1999.

[2] J. M. Ong and L. da Cruz, "The bionic eye: A review," *Clin. Exp. Ophthalmol.*, vol. 40, no. 1, pp. 6–17, 2012.

[3] W. Li, "Integrated retinal implants," Ph.D. dissertation, Dept. Eng. Appl. Sci., California Inst. Technol., Pasadena, CA, USA, 2009.

[4] D. Ng, S. Bai, J. Yang, N. Tran, and E. Skafidas, "Wireless technologies for closed-loop retinal prostheses," *J. Neural Eng.*, vol. 6, art. no. 65004, 2009, doi:10.1088/1741-2560/6/6/065004.

[5] W. C. Ho, C. K. Lee, S. Y. R. Hui, and H. Chung, "Electronic control method for a planar inductive battery charging apparatus," US Patent 8 228 025, Jul. 24, 2012.

[6] G. A. Covic and J. T. Boys, "Modern trends in inductive power transfer for transportation applications," *IEEE J. Emerg. Sel. Topics Power Electron.*, vol. 1, no. 1, pp. 28–41, Mar. 2013.

[7] J. Huh, S. W. Lee, W. Y. Lee, G. H. Cho, and C. T. Rim, "Narrow-width inductive power transfer system for online electrical vehicles," *IEEE Trans. Power Electron.*, vol. 26, no. 12, pp. 3666–3679, Dec. 2011.

[8] H. N. Pham, H. Fujita, K. Ozaki, and N. Uchida, "Estimating method of heat distribution using 3-D resistance matrix for zone-control induction heating systems," *IEEE Trans. Power Electron.*, vol. 27, no. 7, pp. 3374–3382, Jul. 2012.

[9] W. H. Ko, S. P. Liang, and C. D. Fung, "Design of radio-frequency powered coils for implant instruments," *Med. Biol. Eng. Comput.*, vol. 15, no. 6, pp. 634–640, Nov. 1977.

[10] K. M. Silay, D. Dondi, L. Larcher, M. Declercq, L. Benini, Y. Leblebici, and C. Dehollain, "Load optimization of an inductive power link for remote powering of biomedical implants," in *Proc. IEEE Int. Symp. Circuits Syst.*, 2009, pp. 533–536.

[11] W. Zhang, S. C. Wong, C. K. Tse, and Q. Chen, "Analysis and comparison of secondary series- and parallel-compensated inductive power transfer systems operating for optimal efficiency and load-independent voltage-transfer ratio," *IEEE Trans. Power Electron.*, vol. 29, no. 6, pp. 2979–2990, Jun. 2014.

[12] D. Yates, A. Holmes, and A. Burdett, "Optimal transmission frequency for ultralow-power short-range radio links," *IEEE Trans. Circuits Syst. I, Reg. Papers*, vol. 51, no. 7, pp. 1405–1413, Jul. 2004.

[13] M. Pinuela, D. Yates, S. Lucyszyn, and P. Mitcheson, "Maximizing DC-to-load efficiency for inductive power transfer," *IEEE Trans. Power Electron.*, vol. 28, no. 5, pp. 2437–2447, May 2013.

[14] K. Fotopoulou and B. Flynn, "Wireless power transfer in loosely coupled links: Coil misalignment model," *IEEE Trans. Magn.*, vol. 47, no. 2, pp. 416–430, Feb. 2011.

[15] R. Puers, K. van Schuylenbergh, M. Catrysse, and B. Herman, "Wireless inductive transfer of power and data," in *Analog Circuit Design*. New York, NY, USA: Springer, 2006, pp. 395–414.

[16] B. Cannon, J. Hoburg, D. Stancil, and S. Goldstein, "Magnetic resonant coupling as a potential means for wireless power transfer to multiple small receivers," *IEEE Trans. Power Electron.*, vol. 24, no. 7, pp. 1819–1825, Jul. 2009.

[17] X. Liu and S. Hui, "Optimal design of a hybrid windings structure for planar contactless battery charging platform," *IEEE Trans. Power Electron.*, vol. 23, no. 1, pp. 455–463, Jan. 2008.

[18] P. Raval, D. Kacprzak, and A. Hu, "Chapter 7: Technology overview and concept of wireless charging systems," in *Wireless Power Transfer*, J. I. Agbinya, Ed. Aalborg, Denmark: River Publishers, 2012.

[19] B. Lenaerts and R. Puers, "Chapter 5: Omnidirectional coupling," in *Omnidirectional Inductive Powering for Biomedical Implants*. New York, NY, USA: Springer Sci., 2009.

[20] A. RamRakhyani, S. Mirabbasi, and M. Chiao, "Design and optimization of resonance-based efficient wireless power delivery systems for biomedical implants," *IEEE Trans. Biomed. Circuits Syst.*, vol. 5, no. 1, pp. 48–63, Feb. 2011.

[21] M. Kiani, U. Jow, and M. Ghovanloo, "Design and optimization of a 3-coil inductive link for efficient wireless power transmission," *IEEE Trans. Biomed. Circuits Syst.*, vol. 5, no. 6, pp. 579–591, Dec. 2011.

[22] A. K. RamRakhyani and G. Lazzi, "On the design of efficient multi-coil telemetry system for biomedical implants," *IEEE Trans. Biomed. Circuits Syst.*, vol. 7, no. 1, pp. 11–23, Feb. 2013.

[23] M. Ghovanloo and S. Atluri, "A wide-band power-efficient inductive wireless link for implantable microelectronic devices using multiple carriers," *IEEE Trans. Circuits Syst. I, Reg. Papers*, vol. 54, no. 10, pp. 2211–2221, Oct. 2007.

[24] H. Matsumoto, Y. Neba, K. Ishizaka, and R. Itoh, "Model for a three-phase contactless power transfer system," *IEEE Trans. Power Electron.*, vol. 26, no. 9, pp. 2676–2687, Sep. 2011.

[25] J. P. C Smeets, T. T. Overboom, J. W. Jansen, and E. A. Lomonova, "Comparison of position-independent contactless energy transfer systems," *IEEE Trans. Power Electron.*, vol. 28, no. 4, pp. 2059–2067, Apr. 2013.

[26] S. Raabe and G. Covic, "Practical design considerations for contactless power transfer quadrature pick-ups," *IEEE Trans. Ind. Electron.*, vol. 60, no. 1, pp. 400–408, Jan. 2013.

[27] A. Zaheer, G. Covic, and D. Kacprzak, "A bipolar pad in a 10-kHz 300W distributed IPT system for AGV applications," *IEEE Trans. Ind. Electron.*, vol. 61, no. 7, pp. 3288–3301, Jul. 2013.

[28] M. A. Bahmani, T. Thiringer, and H. Ortega, "An accurate pseudoempirical model of winding loss calculation in HF foil and round conductors in switchmode magnetics," *IEEE Trans. Power Electron.*, vol. 29, no. 8, pp. 4231–4246, Oct. 2013.

[29] J. Chow, N. Chen, H. Chung, and L. Chan, "Misalignment tolerable coil structure for biomedical applications with wireless power transfer," in *Proc. 35th Annu. Int. Conf. IEEE Eng. Med. Biol. Soc.*, Osaka, Japan, July 3–7, 2013, pp. 775–778.

[30] F. W. Grover, *Inductance Calculations*. New York, NY, USA: Dover, 2004.

[31] J. I. Agbinya, *Wireless Power Transfer*. Aalborg, Denmark: River Publishers, 2012, ch. 4, p. 119.

[32] L. Wu, Z. Yang, E. Basham, and W. Liu, "An efficient wireless power link for high voltage retinal implant," in *Proc. IEEE Biomed. Circuits Syst. Conf.*, 2008, pp. 101–104.

[33] M. S. Humayun, J. D. Dorn, L. da Cruz, G. Dagnelie, J.-A. Sahel, P. E. Stanga, A. V. Cideciyan, J. L. Duncan, D. Eliott, E. Filley, A. C. Ho, A. Santos, A. B. Safran, A. Arditi, L. V. Del Priore, and, R. J. Greenberg, "Interim results from the international trial of second sight's visual prosthesis," *Ophthalmology*, vol. 119, no. 4, pp. 779–788, Jan. 2012.

[34] G. Wang, W. Liu, M. Sivaprakasam, M. Zhou, J. Weiland, and M. Humayun, "A dual band wireless power and data telemetry for retinal prosthesis," in *Proc. 28th Annu. Int. Conf. IEEE Eng. Med. Biol. Soc.*, Aug. 30–Sep. 3, 2006, pp. 4392–4395.

Jeff Po Wa Chow (S'12) was born in Hong Kong in 1988. He received the B.Eng. degree (Hons.) in electronic engineering from the City University of Hong Kong, Kowloon, Hong Kong, in 2012, where he is currently working toward the Ph.D. degree in power electronics.

His current research is focusing on wireless inductive link.

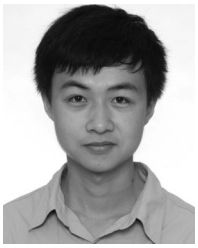

Nan Chen (S'09–M'12) was born in China. He received the B.S. and M.S. degrees in electrical engineering from the Huazhong University of Science and Technology, Wuhan, China, in 2006 and 2008, respectively, and the Ph.D. degree from the City University of Hong Kong, Kowloon, Hong Kong, in 2012.

In February–August 2011, he was an intern student at ABB Corporate Research Center, Switzerland. In May–August 2012, he was a Senior Research Assistant at the City University of Hong Kong. He has published more than ten technical papers and filed six patents. His research interests include the lighting system, power-factor correction preregulators, resonant converters, and grid-connected inverter.

He is currently a Scientist at ABB AB, Corporate Research Center, Västerås, Sweden.

Dr. Chen is also the committee member of the IEEE Power Electronics Society Technical Committee on High-Performance and Emerging Technologies.

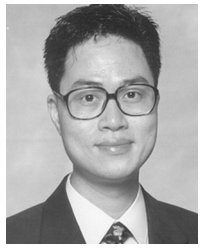

Henry Shu Hung Chung (M'95–SM'03) received the B.Eng. and Ph.D. degrees in electrical engineering both from The Hong Kong Polytechnic University, Hung Hom, Hong Kong, in 1991 and 1994, respectively.

Since 1995, he has been with the City University of Hong Kong, Kowloon, Hong Kong. He is currently a Professor of the Department of Electronic Engineering and the Director of the Centre for Smart Energy Conversion and Utilization Research. He has authored six research book chapters, and more than 338 technical papers including 155 refereed journal papers in his research areas, and holds 32 patents. His research interests include time- and frequency-domain analysis of power electronic circuits, switched-capacitor-based converters, random-switching techniques, control methods, digital audio amplifiers, soft-switching converters, and electronic ballast design.

Dr. Chung is currently an Editor-in-Chief of the IEEE POWER ELECTRONICS LETTERS, and an Associate Editor of the IEEE TRANSACTIONS ON POWER ELECTRONICS, and the IEEE JOURNAL OF EMERGING AND SELECTED TOPICS IN POWER ELECTRONICS.

Leanne Lai Hang Chan (S'07–M'11) received the B.Eng. degree in electrical and electronic engineering from the University of Hong Kong, Pok Fu Lam, Hong Kong, in 2002, and the M.S. degree in electrical engineering and the Ph.D. degree in biomedical engineering both from the University of Southern California, Los Angeles, CA, USA, in 2004 and 2009, respectively.

She joined the Saban Research Institute Neuroscience Program at Children's Hospital Los Angeles in 2009 as a Postdoctoral Associate. Since 2011, she has been with the City University of Hong Kong, Kowloon, Hong Kong. She is an Assistant Professor of the Department of Electronic Engineering. Her research interests include retinal prostheses, electrical stimulation of retina, visually and electrically evoked responses, small animal *in vivo* electrophysiology, microelectrode technology, implantable electronic systems, computer vision and systems biology.

Dr. Chan is a Member of IEEE Engineering in Medicine and Biology Society and Society for Neuroscience.